Formalism for Primordial Black Hole Formation in Spherical Symmetry

Jolyon K. Bloomfield,[1,*] Daniel A. Bulhosa Solórzano,[1,†] and Stephen H. P. Face[1,‡]

[1] *Center for Theoretical Physics, Laboratory for Nuclear Science, and Department of Physics, Massachusetts Institute of Technology, Cambridge, MA 02139, USA*

(Dated: June 2, 2020)

We present a comprehensive formalism for the description of primordial black hole formation in spherical symmetry based on the formalisms of Misner, Sharp, and Hernandez, which can be used to predict whether or not a black hole will form, and extract the resulting black hole mass when formation does occur. Rigorous derivations of all aspects of the formalism are provided, including a thorough investigation of appropriate initial and boundary conditions. We connect our formalism with numerous other approaches in the literature. Some implementation details for numerical code are provided. We include animations of simulated primordial black hole formation as supplemental material. FIXME: Rewrite abstract

PACS numbers: 04.25.dg, 04.40.Nr, 04.70.-s, 98.80.-k

I. INTRODUCTION

FIXME: Update abstract

The very early universe is understood to consist of a generally isotropic and homogeneous plasma with small perturbations. These perturbations, thought to originate in quantum fluctuations driven outside the horizon during inflation [1, 2], form the seeds of structure that give rise to the cosmic microwave background and ultimately the universe as we know it today.

If the primordial perturbations are sufficiently large, it is possible that they might collapse under their own gravity, forming primordial black holes [3, 4]. This requires perturbations to grow to nonlinear scales. The standard inflationary tale predicts Gaussian scale invariant perturbations with amplitudes $\sim 10^{-5}$, meaning that the probability of forming a nonlinear perturbation is negligible; indeed, primordial black hole production rates are predicted to be vanishingly small in this picture [5]. It is conceivable, however, that there exist features in the inflationary power spectrum at small wavelengths, well below cosmic microwave background radiation scales, that may allow perturbations to become sufficiently nonlinear as to grow under their own gravity and undergo gravitational collapse [6–8] (alternatively, large non-Gaussianities or isocurvature may also provide the necessary conditions).

The idea of primordial black holes, whilst currently strictly hypothetical, is intriguing for a number of reasons. Astrophysically, an appropriate spectrum of primordial black holes may provide the seeds for the supermassive black holes found in the centers of galaxies [9]. An entirely different spectrum consisting primarily of lunar mass black holes may be able to explain cold dark matter [10]. Smaller black holes are also of theoretical interest as a window into the process of black hole evaporation through Hawking radiation [11]. Finally, should primordial black holes be identified, this would give insight into the small-scale structure of the very early universe, well beyond what the CMB and large scale structure can provide.

The concept of primordial black holes was first introduced by Zel'dovich and Novikov [12] in 1966, and again by Hawking in 1971 [13]. Theoretical work in the 1970's identified rough criteria for primordial black holes to form [14, 15], and early numerical hydrodynamic simulations were undertaken later that decade [16–18]. Later work investigated the possibility of primordial black hole formation through exotic processes such as bubble collisions [19], cosmic strings [20, 21] and phase transitions [22].

A large amount of work has gone into computing the number density and mass spectrum of primordial black holes from inflationary models [5, 7, 8, 23], and there exists an extensive literature constraining the mass spectrum through astronomical, astrophysical and cosmological measurements [24–29] (see also [30–32] for reviews). The absence of primordial black holes has in turn been used to place constraints on other cosmological processes.

In this paper, we are concerned with the formation of primordial black holes through inflationary perturbations in the primordial plasma. Most work in the literature deals with spherically symmetric perturbations, and we follow this trend. This simplification is justified by the result from peaks theory [33] that the largest peaks resulting from an appropriate probability distribution have a very strong tendency to be (almost) spherical.

In order to understand the primordial black hole number density and mass spectrum, one needs to know the threshold under which perturbations will form primordial black holes. Early work by Carr [14, 15] considered a collapsing region described by a closed Friedmann-Robertson-Walker (FRW) spacetime surrounded by a flat FRW universe. In the radiation-dominated era, this was found to lead to a threshold value for the perturbation amplitude $\delta_c \sim 1/3$, where δ is defined to be the fractional mass

* jolyon@mit.edu
† dbulhosa@mit.edu
‡ face@mit.edu

excess inside the cosmological horizon when the overdense region enters the horizon.

Early hydrodynamical simulations of primordial black hole formation [16, 18] were based on the Misner-Sharp formalism [34], which describes the gravitational collapse of a thermodynamic fluid under spherical symmetry. This formalism cannot evolve past the formation of a black hole, however. To our knowledge, the first numerical evolution capable of extracting the final state black hole mass was Niemayer and Jedamzik [35], who modified stellar collapse code [36] based upon the Hernandez-Misner formalism [37], which uses a null slicing condition to avoid singularity formation. Alternative formalisms have also been proposed [38–40]. A number of works have used these formalisms to investigate critical phenomena and shock formation near the threshold of black hole formation [41–44].

Niemayer and Jedamzik found that the critical mass overdensity $\delta_c \sim 0.7$, much larger than had been previously thought. However, Sasaki and Shibata [38] pointed out that this was due to their initial conditions containing an unphysical decaying mode. Musco *et al.* [45] investigated this further, arriving at a more modest $\delta_c \sim 0.4$. This issue gave rise to investigations of how to construct appropriate initial conditions for numerical simulations. A particularly nice method has been presented by Polnarev *et al.* [46, 47].

While the formation condition for a primordial black hole is known to be roughly $\delta_c \sim 0.4$, the precise value is dependent upon the density profile of the perturbation [48]. Polnarev *et al.* [49, 50] have recently constructed a new criteria which aims to capture the effect of the perturbation profile dependence on the black hole formation condition.

The purpose of this paper is to present a comprehensive formalism for the numerical evolution of spherically symmetric perturbations in the early universe under the influence of their own gravity. We employ the Misner-Sharp [34] and Hernandez-Misner [37] formalisms, building upon the ideas of Niemayer and Jedamzik [35] and Polnarev *et al.* [46, 47]. Our primary goal is to establish a clean and precise formalism from a somewhat murky literature.

Our numerical formalism, while building on previous results, is entirely new. We correct errors in the literature and present new techniques to improve accuracy in simulations. We analyze the regime of validity of various approximations, and provide a concrete description for how to connect inflation to initial conditions for numerical evolution. We have taken pains to be as rigorous and complete as possible, presenting our derivations in a pedagogical manner. We do not give details of a particular numerical implementation, but point to issues that can lead to numerical troubles where appropriate.

FIXME PARAGRAPH: This paper is structured as follows. We begin by deriving the Misner-Sharp formalism in detail in Section II. In Section III, we apply the Misner-Sharp formalism to cosmology, and find variables more appropriate for this evolution. We pay particular attention to the black hole formation condition and appropriate cosmological boundary conditions. Section IV addresses the subject of initial conditions in detail. We then derive the Hernandez-Misner formalism in Section V, and cast it into variables more suited for cosmological evolution in Section **??**. We discuss various coding issues in Section VI. Those who are only interested in seeing the supplemental animations may like to skip to Section VII, where we demonstrate and explain simulations in our formalism. Finally, we conclude in Section VIII. A number of technical appendices are included.

II. MISNER-SHARP FORMALISM

We begin by investigating Einstein's equations for a spacetime containing a perfect fluid under the assumption of spherical symmetry. We follow the formalism first laid out by Misner and Sharp [34], and aim to present a detailed but concise derivation of the equations of motion.

A spacetime is spherically symmetric if it possesses an $SO(3)$ isometry (3D rotation) group, where the action of this group on any given point (the 'orbits' of the group) are two-dimensional spheres [51]. The spacetime metric induces a two-dimensional metric on each such sphere, which must be proportional to the metric of a unit two-sphere,

$$d\Omega^2 = d\theta^2 + \sin^2\theta \, d\phi^2 \tag{1}$$

for two coordinates θ and ϕ. This two-dimensional metric possesses three Killing vectors, associated with rotations around three axes. Demanding that the spacetime metric also possess these Killing vectors constrains it to take the form

$$ds^2 = g_{AB}dx^A dx^B + R^2(x^A)d\Omega^2 \tag{2}$$ eq:smetric

where x^0 and x^1 are arbitrary coordinates and the two-dimensional metric g_{AB} depends only on x^0 and x^1. The remaining gauge freedom in this metric lies in redefinitions of x^0 and x^1.

We describe the matter content of the spacetime as a perfect fluid with stress-energy tensor

$$T_{\mu\nu} = (\rho + P)u_\mu u_\nu + P g_{\mu\nu} \tag{3}$$ eq:perfluid

where ρ is the energy density, P is the pressure, and u^μ is the four-velocity of the fluid. Note that because this tensor is diagonal in the local rest frame of the fluid, it cannot describe the energy flow associated with radiation [34]. In particular, this means that free-streaming neutrinos cannot be described in this formalism. We discuss the use of a perfect-fluid description of the early universe photon bath in Appendix A.

To describe the fluid, we employ coordinates that move with the fluid, known as comoving or Lagrangian coordinates. In such coordinates, only the time-like component

u^0 of the fluid four-velocity is nonzero. While maintaining comoving coordinates, we have sufficient remaining gauge freedom to choose the metric to be diagonal, $g_{01} = 0$. Naming the timelike coordinate t and the spacelike radial coordinate A, we write the metric as

$$ds^2 = -e^{2\phi}dt^2 + e^{\lambda}dA^2 + R^2 d\Omega^2 . \tag{4}$$ eq:MSmetric

Here ϕ, λ, and R can all be functions of A and t. The fluid four-velocity is given by

$$u^t = e^{-\phi}, \qquad u^A = u^\theta = u^\phi = 0 . \tag{5}$$

The remaining gauge freedom lies solely in reparameterizations of the form $t = t(\tilde{t})$ and $A = A(\tilde{A})$. For convenience, we choose A such that $A = 0$ is the coordinate about which space is spherically symmetric, with $R(t, 0) = 0$.

The preliminaries complete, we now compute the equations of motion. We begin with the Einstein equation $G_{\mu\nu} = 8\pi T_{\mu\nu}$, where we work with $G = c = 1$. The time-time, radius-radius, and time-radius components of the equation are as follows, where we use primes and overdots to denote derivatives with respect to A and t respectively.

$$8\pi e^{2\phi}\rho = \frac{1}{R^2}\left(e^{2\phi} + \dot{R}^2 - e^{-\lambda+2\phi}(R')^2\right) + \frac{e^{-\lambda}}{R}\left(e^{\lambda}\dot{R}\dot{\lambda} + e^{2\phi}R'\lambda' - 2e^{2\phi}R''\right) \tag{6a}$$ eq:Einsteintt

$$8\pi e^{\lambda}P = \frac{1}{R^2}\Big[(R')^2 + 2RR'\phi' - e^{\lambda-2\phi}(e^{2\phi} + \dot{R}^2 - 2R\dot{R}\dot{\phi} + 2R\ddot{R})\Big] \tag{6b}$$ eq:Einsteinrr

$$0 = \frac{\dot{\lambda}R' + 2\dot{R}\phi' - 2\dot{R}'}{R} \tag{6c}$$ eq:Einsteintr

Except for the $\theta\theta$ and $\phi\phi$ components, all other components of the Einstein equation vanish identically. The $\theta\theta$ and $\phi\phi$ components are related by symmetry, and as the Einstein equation and the conservation of stress-energy equation are related by the Bianchi identity, these angular components can be neglected in favor of the simpler equations arising from conservation of stress-energy.

We now use conservation of stress-energy, $\nabla_\mu T^{\mu\nu} = 0$. The t and A components are

$$0 = 2R\dot{\rho} + (P + \rho)(4\dot{R} + \dot{\lambda}R) \tag{7a}$$ eq:stresst

$$0 = P' + (\rho + P)\phi' \tag{7b}$$ eq:stressr

while the θ and ϕ components vanish identically.

The following definitions allow us to bring the equations of motion into a more convenient form.

$$U = e^{-\phi}\dot{R} \tag{8a}$$ eq:Udef

$$\Gamma = e^{-\lambda/2}R' \tag{8b}$$ eq:Gammadef

$$m = 4\pi\int_0^A \rho R^2 R' dA \tag{8c}$$ eq:mdef

U is the coordinate velocity of a fluid element, as the fluid element at comoving radius A is positioned at radius R. Note that this is only a coordinate velocity, not a physical velocity, and therefore can exceed unity. The quantity Γ measures the rate at which R increases in a reparametrization-invariant manner. The quantity m is the Misner-Sharp mass, a measure of the gravitational mass contained within the coordinate radius A. The following related expressions are useful.

$$e^{-\phi}\ddot{R} = \dot{U} + U\dot{\phi} \tag{9a}$$ eq:rdotdot

$$e^{-\lambda/2}R'' = \Gamma' + \frac{1}{2}\Gamma\lambda' \tag{9b}$$ eq:rprimeprime

$$m' = 4\pi R^2 R'\rho \tag{9c}$$ eq:MSmprime

We now construct the Misner-Sharp equations of motion using these definitions. Begin by solving Eq. (7b) for ϕ'.

$$\phi' = -\frac{P'}{\rho + P} \tag{10}$$ eq:phiprime

Next, write Eq. (6c) as

$$\dot{\lambda}R' = 2(\dot{R}' - \dot{R}\phi') , \tag{11a}$$ eq:lambdadot

$$\dot{\lambda} = \frac{2e^{\phi}U'}{R'} . \tag{11b}$$ eq:lambdadot2

Take Eq. (6a) and substitute in Eqs. (8a), (8b), (9b) and (11b) to obtain

$$8\pi\rho R^2 R' = \frac{d}{dA}\left((1 + U^2 - \Gamma^2)R\right) . \tag{12}$$

Integrating this from 0 to A, imposing the boundary condition $R(t, 0) = 0$, and using Eq. (8c) we find

$$\Gamma^2 = 1 + U^2 - \frac{2m}{R} . \tag{13}$$ eq:MSGamma

Now, multiply Eq. (7a) by $2\pi RR'$ and substitute Eq. (11a). Some rearrangement leads to

$$0 = \frac{d}{dt}\left(4\pi\rho R^2 R'\right) + 4\pi\frac{d}{dA}\left(PR^2\dot{R}\right) . \tag{14}$$ eq:stresst2

Integrate this over the radial coordinate from 0 to A, then make use of Eqs. (8a) and (8c) to obtain

$$\dot{m} = -e^{\phi}4\pi R^2 PU \tag{15}$$ eq:MSmdot

where we once again employ the boundary condition $R(t, 0) = 0$. The last equation comes from Eq. (6b). Substituting Eqs. (8a), (8b) and (9a) yields

$$2e^{-\phi}R\dot{U} = \Gamma^2 - 1 - U^2 + 2\Gamma^2 R\frac{\phi'}{R'} - 8\pi PR^2 . \tag{16}$$

This can be further simplified using Eqs. (10) and (13).

$$\dot{U} = -e^{\phi}\left(\Gamma^2\frac{P'}{R'(\rho + P)} + \frac{m + 4\pi PR^3}{R^2}\right) \tag{17}$$ eq:MSUdot

We now have the six equations that constitute the Misner-Sharp formalism [34]. Three equations are evolution equations for R, m and U (Eqs. (8a), (15) and (17)), and three equations are constraint equations for ρ, ϕ and Γ (Eqs. (9c), (10), and (13)). Together, they express the content of Einstein's equations in a convenient manner for numerical implementation.

This system of equations must be supplemented by an equation of state P. In the original Misner-Sharp formalism, the equation of state was taken to depend on energy density and specific energy (kinetic energy density), and so thermodynamic relations were also required to close the system of equations. For early universe cosmology purposes, we can take pressure to be a function of energy density only, and so we only need the equation of state[1] $P = w\rho$.

Because it describes fluid flows, the Misner-Sharp formalism has the capacity to develop shocks. A typical way to combat this is to introduce an artificial viscosity term into the equations in order to smooth out any shocks [52]. The effect of adding a viscous term is to let pressure $P = P_0 + Q$, where P_0 is the physical pressure and Q is the artificial viscosity. For the moment, we include a viscous term as Q in the equations of motion, and leave a detailed discussion of viscosity for Section VI. For the physical pressure, we will use $P_0 = w\rho$, where w is the (possibly time-dependent) equation of state. For radiation, $w = 1/3$, as we detail in Appendix A.

We complete the formalism by specifying boundary conditions. We already chose $R(t, 0) = 0$ as the center of spherical symmetry. By the definitions of U and m, we then have $U(t, 0) = m(t, 0) = 0$. By spherical symmetry, ϕ must be even around the origin, and combined with the fact that the field equations demand that ϕ'' be defined at the origin, we must have $\phi'(t, 0) = 0$. Equation (10) then demands that $P'(t, 0) = 0$. Generally speaking, a cusp in the density ρ is permitted at the origin, but for equation of state $P = w\rho$, we must also have $\rho'(t, 0) = 0$. Using L'Hôpital's Rule, we find that

$$\lim_{A\to 0} \Gamma^2 = 1 - \lim_{A\to 0} \frac{8\pi\rho R^2 R'}{R'} = 1\,. \tag{18}$$

Our equations must be supplemented with a boundary condition for ϕ (corresponding to a gauge condition on the time coordinate), and a boundary condition for U, m or ρ (to control the incoming fluid characteristic).

Initial conditions at time t_0 must be set for each of the evolution variables, namely $m(t_0, A)$ (or equivalently, $\rho(t_0, A)$), $U(t_0, A)$ and $R(t_0, A)$. The first two of these correspond to the local energy density and fluid velocity, while the third of these is the initial gauge condition (note that by reparametrization invariance, it is perfectly fine to choose $R(t_0, A) = A$). The fluid provides the only dynamical degree of freedom; the gauge condition simply evolves with time as dictated by the fluid.

We now summarize the Misner-Sharp equations for convenience.

$$\dot{R} = Ue^{\phi} \tag{19a}$$

$$\dot{m} = -e^{\phi} 4\pi R^2 PU \tag{19b}$$

$$\dot{U} = -e^{\phi}\left(\frac{\Gamma^2 P'}{R'(\rho + P)} + \frac{m}{R^2} + 4\pi RP\right) \tag{19c}$$

$$\rho = \frac{m'}{4\pi R^2 R'} \tag{19d}$$

$$\phi' = -\frac{P'}{\rho + P} \tag{19e}$$

$$\Gamma^2 = 1 + U^2 - \frac{2m}{R} \tag{19f}$$

For convenience, we also note that

$$\dot{\rho} = -e^{\phi}(\rho + P)\left(2\frac{U}{R} + \frac{U'}{R'}\right) \tag{20}$$

as can be quickly derived from Eqs. (7a) and (11b). It is worth noting that these equations of motion reflect the reparametrization invariance of t and A, with spatial derivatives appearing in ratios and time derivatives appearing in terms of the reparametrization-invariant combination $e^{-\phi}\partial_t$.

When artificial viscosity is turned off and w is constant, we can integrate Eq. (19e) to obtain

$$e^{\phi} = \left(\frac{\rho_{\rm ref}}{\rho}\right)^{w/(1+w)} \tag{21}$$

where $\rho_{\rm ref}(t)$ is some reference density which provides the boundary condition on ϕ.

III. COSMOLOGICAL APPLICATION OF THE MISNER-SHARP FORMALISM

The Misner-Sharp formalism was originally designed to study stellar collapse, where the stress-energy tensor vanishes after some radius and the metric beyond this is simply the Schwarzschild metric. In cosmology, the stress energy tensor doesn't vanish anywhere, and spacetime is not asymptotically flat: the "background solution" we require is a Friedmann-Robertson-Walker (FRW) solution instead of a Schwarzschild solution. In this section, we use the Misner-Sharp formalism derived above to describe cosmological evolution by investigating the Friedmann-Robertson-Walker (FRW) limit. We then recast the Misner-Sharp formalism into variables that are better suited to describing evolution on a cosmological background.

[1] A number of papers in the primordial black hole literature employ thermodynamic relations in their system of equations despite this. To our knowledge, this is unnecessary.

A. Background Evolution

We begin by exploring the background cosmological evolution, where we take $P = w\rho$ with possibly time-dependent w. Homogeneity requires that the energy density and pressure are constant in space, yielding $P_b' = \rho_b' = 0$, where the subscript b indicates the background FRW value. This in turn leads to $\phi_b' = 0$ from Eq. (19e) (we ignore artificial viscosity for this calculation). By choosing $\rho_{\rm ref} = \rho_b$, we can set $\phi_b = 0$[2]. Equation (19d) can now be integrated to obtain

$$m_b = \frac{4\pi}{3}\rho_b R_b^3 \,. \tag{22}$$

Using these results, the evolution equations (19a), (19b) and (19c) become the following.

$$\dot{R}_b = U_b \tag{23a}$$

$$\dot{\rho}_b = -3\frac{\dot{R}_b}{R_b}\rho_b(1+w) \tag{23b}$$

$$\dot{U}_b = -\frac{4\pi}{3}\rho_b R_b(1+3w)\,. \tag{23c}$$

In particular, note that there are no spatial derivatives here, and so the evolution of each function will be independent of A. This allows us to write $R_b(A,t) = a(t)R_0(A)$, where $a(t)$ is the usual scale factor of FRW cosmology. Substituting this into the equations of motion then yields the following.

$$U_b = \dot{a}R_0 \tag{24a}$$

$$\dot{\rho}_b = -3\frac{\dot{a}}{a}\rho_b(1+w) \tag{24b}$$

$$\dot{U}_b = -\frac{4\pi}{3}\rho_b a R_0(1+3w) \tag{24c}$$

The second of these is recognizable as the continuity equation in cosmology. The other two combine to yield the acceleration equation,

$$\frac{\ddot{a}}{a} = -\frac{4\pi}{3}\rho_b(1+3w). \tag{25}$$

Combining the continuity equation and the acceleration equation yields

$$\frac{d}{dt}(\dot{a}^2) = \frac{8\pi}{3}\frac{d}{dt}(\rho_b a^2) \tag{26}$$

which integrates to give the Friedmann equation

$$\left(\frac{\dot{a}}{a}\right)^2 \equiv H^2 = \frac{8\pi}{3}\rho_b - \frac{k}{a^2} \tag{27}$$

with spatial curvature k appearing as a constant of integration. We can multiply this by R_0^2 and substitute for U_b to obtain

$$U_b^2 = \frac{2m_b}{R_b} - kR_0(A)^2 \tag{28}$$

and thus

$$\Gamma_b^2 = 1 - kR_0(A)^2\,. \tag{29}$$

Note that this means Γ_b must be time-independent. From the definition of Γ, we have

$$\Gamma_b = e^{-\lambda/2}aR_0'(A) \tag{30}$$

and so $e^{-\lambda/2} \propto 1/a$. Using reparametrization invariance of A, we're free to choose $e^{-\lambda/2} = 1/a$, which then requires

$$(R_0')^2 = 1 - kR_0^2. \tag{31}$$

The solutions to this differential equation are

$$R_0(A) = \begin{cases} \frac{1}{\sqrt{k}}\sin(\sqrt{k}A) & k > 0 \\ A & k = 0 \\ \frac{1}{\sqrt{-k}}\sinh(\sqrt{-k}A) & k < 0, \end{cases} \tag{32}$$

and the metric is then simply the appropriately-curved FRW metric

$$ds^2 = -dt^2 + a(t)^2\left(dA^2 + R_0(A)^2 d\Omega^2\right). \tag{33}$$

Thus, the Misner-Sharp equations yield the general FRW cosmological evolution, as expected.

It is interesting to note that the quantities R and m are not required to be monotonic, as demonstrated by the closed FRW solution. However, for universes where $R(t,\infty) = \infty$, non-monotonicity in these variables requires an Einstein-Rosen bridge, which if not present in the initial data, will not form. For the remainder of this paper, we assume that R and m are monotonically increasing, which in turn implies that $\Gamma > 0$.

Let us specialize to the case of $k = 0$ (flat FRW) with constant equation of state w. As we aim to model cosmological evolution in the radiation dominated era immediately after inflation has suppressed all spatial curvature, this is a reasonable regime to investigate. We use reparametrization invariance to take $a(t_0) = 1$.

We solve the background cosmological evolution as follows. The continuity equation is integrated to obtain

$$\rho_b = \rho_0 a^{-3(1+w)} \tag{34}$$ eq:rhosol

where $\rho_b(t_0) = \rho_0$. The Friedmann equation then becomes

$$\dot{a} = \sqrt{\frac{8\pi\rho_0}{3}}a^{1-1/\alpha} \tag{35}$$

[2] This selects cosmological time as the time coordinate; introducing appropriate powers of the cosmological scale factor into $\rho_{\rm ref}$ can instead select conformal time.

where we have defined $\alpha = 2/(3(1+w))$ for convenience, assuming $w > -1$ ($\alpha = 1/2$ for $w = 1/3$). This can be integrated to obtain

$$\alpha(a^{1/\alpha} - 1) = \sqrt{\frac{8\pi\rho_0}{3}}(t - t_0)\,. \tag{36}$$

Choosing the singularity $a = 0$ to occur at $t = 0$, we obtain

$$t_0 = \alpha\sqrt{\frac{3}{8\pi\rho_0}} \tag{37}$$ eq:t0def

which in turn yields

$$a = \left(\frac{t}{t_0}\right)^{\alpha}\,. \tag{38}$$ eq:asol

The Hubble parameter is then given by

$$H = \frac{\alpha}{t}\,. \tag{39}$$

B. Beyond the Background

While the full Misner-Sharp equations describe gravitational collapse in cosmology, they are not written in terms of the most efficient quantities, particularly from a numerical perspective. As we can solve the background evolution exactly, it is useful to factor out this aspect of the solution from the variables. In this subsection, we transform the Misner-Sharp equations in such a manner over a flat cosmological background. This subsection draws upon and improves the ideas of Polnarev, Nakama and Yokoyama [47].

Begin by defining R_H to be the horizon radius at t_0,

$$R_H = \frac{1}{H(t_0)} = \frac{t_0}{\alpha}. \tag{40}$$

This is the appropriate dimensionful scale of the problem, and we use it to de-dimensionalize all of our quantities. In particular, we define $\bar{A} = A/R_H$ to be a dimensionless comoving radius. We further define the following rescaled variables.

$$\rho = \rho_b\tilde{\rho}$$ eq:trhodef (41a)

$$P = \rho_b\tilde{P} = \rho_b\tilde{\rho}(w + \tilde{Q}) \tag{41b}$$

$$R = aR_H\tilde{R}$$ eq:newR (41c)

$$U = HaR_H\tilde{U}$$ eq:newvariablesU (41d)

$$m = \frac{4\pi}{3}\rho_b R^3\tilde{m}$$ eq:newvariablesm (41e)

These rescalings have been chosen to factor out the cosmological expansion of the universe, while retaining the invariance of the equations under spatial reparametrizations. On the background evolution, we have $\tilde{\rho} = \tilde{m} = 1$, $\tilde{P} = w$ and $\tilde{R} = \tilde{U} = \bar{A}$. The quantity $\tilde{Q}$ is a dimensionless form for artificial viscosity. For both $\tilde{R}$ and $\tilde{U}$, we tried scaling out factors of $\bar{A}$, but found this to be unhelpful for both interpretation and implementation. Of these functions, $\tilde{\rho}$, $\tilde{P}$, $\tilde{Q}$ and $\tilde{m}$ are even functions of $\bar{A}$, while $\tilde{U}$ and $\tilde{R}$ are odd.

It is also useful to define a dimensionless time variable. A particularly nice choice is to work in logarithmic time

$$\xi = \ln\left(\frac{t}{t_0}\right) = \frac{1}{\alpha}\ln a \tag{42}$$

which makes quantities that depend on powers of a evolve linearly with ξ. In terms of ξ, we can construct the following useful expressions.

$$\partial_t = \frac{H}{\alpha}\partial_\xi$$ eq:dxi (43a)

$$a = e^{\alpha\xi}$$ eq:axi (43b)

$$H = \frac{\alpha}{t_0}e^{-\xi} = \frac{1}{R_H}e^{-\xi}$$ eq:Hxi (43c)

$$HaR_H = e^{(\alpha-1)\xi} \tag{43d}$$

$$H^2 = \frac{8\pi}{3}\rho_b = \frac{e^{-2\xi}}{R_H^2} \tag{43e}$$

The last of these follows from the Friedmann equation.

Using these definitions, the Misner-Sharp equations become the following.

$$\partial_\xi\tilde{R} = \alpha\left(\tilde{U}e^{\phi} - \tilde{R}\right) \tag{44a}$$

$$\partial_\xi\tilde{m} = 2\tilde{m} - \frac{3\alpha\tilde{U}}{\tilde{R}}e^{\phi}\left(\tilde{P} + \tilde{m}\right) \tag{44b}$$

$$\partial_\xi\tilde{U} = (1-\alpha)\tilde{U} - \alpha e^{\phi}\left[\frac{\bar{\Gamma}^2\tilde{P}'}{\tilde{R}'(\tilde{\rho}+\tilde{P})} + \frac{\tilde{R}}{2}\left(\tilde{m} + 3\tilde{P}\right)\right]$$ eq:newu (44c)

$$\tilde{\rho} = \tilde{m} + \frac{\tilde{R}\tilde{m}'}{3\tilde{R}'}$$ eq:rhomrel (44d)

$$\phi' = -\frac{\tilde{P}'}{\tilde{\rho}+\tilde{P}}$$ eq:phifinal (44e)

$$\bar{\Gamma}^2 = \frac{\Gamma^2}{(HaR_H)^2} = e^{2(1-\alpha)\xi} + \tilde{U}^2 - \tilde{R}^2\tilde{m}$$ eq:newgamma (44f)

Here, we repurpose primes to denote derivatives with respect to $\bar{A}$, and we've made liberal use of the background expressions, the continuity equation and the Friedmann equation. Note that these equations are manifestly invariant under reparametrizations of $\bar{A}$, but no longer for ξ. These equations are supplemented by the boundary conditions $\tilde{R} = \tilde{m}' = \tilde{U} = \tilde{\rho}' = 0$ at $\bar{A} = 0$. When $\tilde{Q} = 0$, we have

$$e^{\phi} = \tilde{\rho}^{-3\alpha w/2}\,.$$ eq:MSphinov (45)

We suggest using this result to provide a boundary condition for ϕ at the outer boundary, which keeps the time

coordinate synchronized with the background FRW cosmological time. We construct an outer boundary condition for $\tilde{U}$ in Section IV. Initial data consists of specifying $\tilde{R}$, $\tilde{m}$ (or $\tilde{\rho}$) and $\tilde{U}$ at time $\xi = 0$.

The equations (44) are the complete dimensionless cosmological Misner-Sharp equations of motion. Note that there is no dependence upon dimensionful constants at all, which implies that for any initial $\tilde{R}$, $\tilde{m}$ and $\tilde{U}$, the evolution will be the same no matter the initial time/density/horizon scale.

It is convenient to note that the horizon scale evolves as

$$R_H(\xi) = \frac{1}{H} = R_H e^{\xi} \tag{46}$$

in areal radius, while the comoving radius $\bar{A}_H$ for the horizon can be found by solving $R(\bar{A}_H) = R_H(\xi)$ to obtain

$$\tilde{R}(\bar{A}_H) = e^{(1-\alpha)\xi}. \tag{47}$$

Recall that on the background, $\tilde{R}(\bar{A}) = \bar{A}$, which gives a good estimate for the horizon location. We will also later need an expression for $\partial_\xi \tilde{\rho}$, which is given by

$$\partial_\xi \tilde{\rho} = 2\tilde{\rho} - \alpha e^{\phi}(\tilde{\rho} + \tilde{P}) \left(\frac{2\tilde{U}}{\tilde{R}} + \frac{\tilde{U}'}{\tilde{R}'} \right). \tag{48}$$ eq:rhouseful

C. Black Hole Formation

We now possess the tools to evolve initial density and velocity profiles. Next, we need a method for detecting the appearance of a black hole. To do this, we search for the creation of an apparent horizon, which if detected, points to the existence of an event horizon[3]. The following results are summarized from §7 of Baumgarte and Shapiro [53].

Define n^a to be the timelike unit vector orthogonal to slices of constant t, and s^a to be the spacelike unit vector orthogonal to slices of constant A. Together, these define an outgoing null vector $k^a = (n^a + s^a)/\sqrt{2}$. In our metric, $k^a = (e^{-\phi}, e^{-\lambda/2}, 0, 0)/\sqrt{2}$.

The expansion of outgoing radial null geodesics is given by $\Theta = m^{ab}\nabla_a k_b$ where $m^{ab} = g^{ab} + n^a n^b - s^a s^b$ is the two-dimensional metric on the hypersurface of constant t and A. An apparent horizon forms when $\Theta \leq 0$. For spherical spacetimes, this yields

$$\Theta = \frac{1}{4\pi R^2} k^a \nabla_a (4\pi R^2). \tag{49}$$

From our metric, we have

$$\Theta = \frac{\sqrt{2}}{R}\left(U + \Gamma\right). \tag{50}$$

As such, an apparent horizon forms when $U + \Gamma \leq 0$. As $\Gamma > 0$, this requires U to be negative. Using Eq. (13), the condition for black hole formation becomes

$$\frac{2m}{R} \geq 1 \tag{51}$$

which is recognizable as requiring an amount of mass inside a radius R that is smaller than its Schwarzschild radius, thus satisfying the hoop conjecture. Using (41e) and the Friedmann equation, this yields

$$\tilde{R}^2 \tilde{m} e^{2(\alpha-1)\xi} \geq 1\,. \tag{52}$$ eq:bhcondition

Thus, one should check for the conditions $\tilde{U} < 0$ and (52) as the conditions under which a black hole forms.

An alternative derivation considers the rate of change of R for an outgoing null ray over time.

$$\frac{dR}{dt} = \frac{\partial R}{\partial t} + \frac{\partial R}{\partial A}\frac{dA}{dt} = e^{\phi}(U + \Gamma) \tag{53}$$

When an outgoing null ray starts heading inwards, an apparent horizon has formed, leading to the same condition as previously.

After the apparent horizon forms, a singularity will form at the origin soon thereafter; the singularity forms once dR/dt at the origin becomes zero. The Misner-Sharp formalism cannot evolve past the formation of a singularity, and so a new technique is needed if more information about the resulting black hole (such as its mass) is desired. This brings us to the Hernandez-Misner formalism, which we introduce in Section V.

IV. LINEAR ANALYSIS

The formalism presented above has evolution equations for $\tilde{m}$, $\tilde{R}$ and $\tilde{U}$, and constraint equations for calculating $\tilde{\rho}$, $\bar{\Gamma}$ and ϕ. As such, initial data for m, R, and U should be specified on a surface of constant t or ξ ($\tilde{m}$ may be substituted for $\tilde{\rho}$ or ϕ if desired). We note that the initial data for $\tilde{R}$ is simply a gauge choice; the physical initial data is $\tilde{m}(R)$ and $\tilde{U}(R)$, describing the fluid energy density and velocity.

It is intended that the initial conditions are initially generated from inflationary perturbations, which undergo linear evolution before re-entering the horizon, after which they may undergo gravitational collapse. Linear fluid perturbations in cosmology are known to have two modes: a growing mode and a decaying mode. In the time between the end of inflation and the beginning of numerical evolution, the decaying mode will undergo decay. As such, initial data chosen close to the time of re-entry should

[3] Note that the lack of an apparent horizon does not necessarily imply that there is no event horizon, but this is typically limited to specific spacetime slicings. For our purposes, we may assume that an apparent horizon will form before the central singularity.

typically be selected so as to consist of the growing mode only. Disregard for this issue affected early work on this subject [35], as pointed out by Shibata and Sasaki [38].

More recently, [46] developed a formulation that selects initial data comprising only a growing mode in the linear regime. This formalism was expanded in [47], and utilized in [49]. However, this formalism can only evolve superhorizon modes.

In this section, we perform a linear analysis of the system in order to evolve modes both inside and outside the horizon in the linear regime. This allows us to propagate initial data (including both growing and decaying modes) from early times to modestly nonlinear scales, at which point nonlinear evolution may take over. This analysis also provides analytic insight into a number of aspects of the system.

A. Linearized Equations of Motion

To linearize our system, we perturb about the cosmological backgrounds as follows, where we use ϵ as an order counting parameter.

$$\tilde{R} = (1+\epsilon\delta_R)\bar{A} \tag{54a}$$
$$\tilde{U} = (1+\epsilon\delta_U)\tilde{R} \approx (1+\epsilon(\delta_U+\delta R))\bar{A} \tag{54b}$$ eq:deltaU
$$\tilde{m} = 1+\epsilon\delta_m \tag{54c}$$ eq:deltam
$$\tilde{\rho} = 1+\epsilon\delta_\rho \tag{54d}$$
$$e^{\phi} = 1+\epsilon\delta_\phi \tag{54e}$$

The only unusual choice here is for the decomposition of $\tilde{U}$, which has been motivated by the background expression $U_b = HR_b$, and the fact that this choice decouples δ_R from the remainder of the system at linear order. It is straightforward to linearize Eqs. (44) from these definitions.

$$\delta_\phi = -\frac{3w\alpha}{2}\delta_\rho \tag{55a}$$ eq:deltaphieq
$$\partial_\xi\delta_R = \alpha\left(\delta_U+\delta_\phi\right) \tag{55b}$$ eq:deltareq
$$\delta_\rho = \delta_m + \frac{\bar{A}}{3}\delta_m' \tag{55c}$$ eq:deltarhoeq
$$\partial_\xi\delta_m = 3\alpha w\delta_m - 2\delta_U - 2\delta_\phi - 3\alpha w\delta_\rho \tag{55d}$$ eq:deltameq
$$\partial_\xi\delta_U = (1-2\alpha)\delta_U - \delta_\phi - \frac{\alpha}{2}\left(\delta_m + 3w\delta_\rho\right) - \frac{3w\alpha^2}{2}\frac{\delta_\rho'}{\bar{A}}e^{2(1-\alpha)\xi} \tag{55e}$$ eq:deltaueqprelim

We can also linearize (48) to find an evolution equation for δ_ρ.

$$\partial_\xi\delta_\rho = -2\delta_\phi - 2\delta_U - \frac{2}{3}\bar{A}\delta_U' \tag{56}$$ eq:rhodxi

Note that δ_R appears only once as $\partial_\xi\delta_R$, justifying our choice of variables.

It is simplest to solve the system in terms of δ_ρ. To do this, we begin by eliminating δ_ϕ from the above equations, writing them in the following form.

$$\delta_\rho = \left(1+\frac{\bar{A}}{3}\partial_{\bar{A}}\right)\delta_m \tag{57a}$$
$$\partial_\xi\delta_U = (1-2\alpha)\delta_U - \frac{\alpha}{2}\delta_m - \frac{3w\alpha^2}{2}\frac{\delta_\rho'}{\bar{A}}e^{2(1-\alpha)\xi} \tag{57b}$$
$$\partial_\xi\delta_\rho = 3w\alpha\delta_\rho - 2\left(1+\frac{\bar{A}}{3}\partial_{\bar{A}}\right)\delta_U \tag{57c}$$ eq:getrhodot
$$\partial_\xi\delta_m = 3\alpha w\delta_m - 2\delta_U \tag{57d}$$ eq:useful

The last of these is not immediately required, but will be useful later. Taking a further time derivative of $\partial_\xi\delta_\rho$, we can substitute for $\partial_\xi\delta_U$ to yield the following.

$$\partial_\xi^2\delta_\rho = 3w\alpha\partial_\xi\delta_\rho + 3w\alpha^2 e^{2(1-\alpha)\xi}\left(1+\frac{\bar{A}}{3}\partial_{\bar{A}}\right)\frac{\delta_\rho'}{\bar{A}} + \alpha\left(1+\frac{\bar{A}}{3}\partial_{\bar{A}}\right)\delta_m - 2(1-2\alpha)\left(1+\frac{\bar{A}}{3}\partial_{\bar{A}}\right)\delta_U \tag{58}$$

We now eliminate the spatial derivatives of δ_m and δ_U using Eqs. (57).

$$\partial_\xi^2\delta_\rho = \frac{\alpha}{2}(9w-1)\partial_\xi\delta_\rho + w\alpha^2 e^{2(1-\alpha)\xi}\left(\frac{2\delta_\rho'}{\bar{A}}+\delta_\rho''\right) + (\alpha-(1-2\alpha)3w\alpha)\delta_\rho \tag{59}$$ eq:rhoddxi2

This is the desired equation of motion. Note that it is separable, and hence can be solved using a mode expansion.

For simplicity, we will proceed with the equation of state for radiation ($w = 1/3$, $\alpha = 1/2$)[4]. In this regime, the equation of motion becomes

$$\partial_\xi^2\delta_\rho = \frac{1}{2}\partial_\xi\delta_\rho + \frac{1}{2}\delta_\rho + \frac{1}{12}e^{\xi}\left(\frac{2\delta_\rho'}{\bar{A}}+\delta_\rho''\right). \tag{60}$$ eq:linearrho

To solve this, it is helpful to let $t = \exp(\xi/2)/\sqrt{3}$, which leads to

$$\partial_t^2\delta_\rho - \frac{2}{t^2}\delta_\rho = \frac{2\delta_\rho'}{\bar{A}} + \delta_\rho''. \tag{61}$$

We now let $\delta_\rho(t,\bar{A}) = \sigma(t)\gamma(\bar{A})$ and separate variables.

$$\frac{1}{\sigma}\left(\partial_t^2\sigma - \frac{2}{t^2}\sigma\right) = \frac{1}{\gamma}\left(\frac{2\gamma'}{\bar{A}}+\gamma''\right) = \lambda \tag{62}$$

This has reduced to a pair of Sturm-Liouville equations.

We begin with the equation for $\gamma(\bar{A})$,

$$\gamma'' + \frac{2\gamma'}{\bar{A}} = \lambda\gamma. \tag{63}$$

[4] Only the time evolution is modified by the choice of w; the spatial mode functions are independent of w.

This equation requires that γ be an eigenfunction of the derivative operator $(2/\bar{A})\partial_{\bar{A}} + \partial^2_{\bar{A}} \equiv \bar{A}^{-2}\partial_{\bar{A}}\bar{A}^2\partial_{\bar{A}}$ with eigenvalue λ. For boundary conditions, we impose $\gamma'(0) = 0$ by symmetry across the origin, and choose $\gamma(\bar{A}_{\rm max}) = 0$. While this is an unphysical reflecting boundary condition, it is useful for understanding the linear analysis, and reflections are minimal when the data near the outer boundary is close to FRW. One can of course take $\bar{A}_{\rm max} \to \infty$ by moving to a continuous description of modes. Consider the integral

$$I = \int_0^{\bar{A}_{\rm max}} d\bar{A}\, \bar{A}^2 \gamma(\bar{A})(\bar{A}^{-2}\partial_{\bar{A}}\bar{A}^2\partial_{\bar{A}})\gamma(\bar{A}). \tag{64}$$

We can integrate by parts to obtain

$$I = -\int_0^{\bar{A}_{\rm max}} d\bar{A}\, \bar{A}^2 (\partial_{\bar{A}}\gamma(\bar{A}))^2 \leq 0 \tag{65}$$

where the boundary terms vanish by the boundary conditions. As γ is an eigenfunction of the derivative operator, we also have

$$I = \lambda \int_0^{\bar{A}_{\rm max}} d\bar{A}\, \bar{A}^2 \gamma(\bar{A})^2. \tag{66}$$

As this integrand is positive semidefinite, we see that $\lambda \leq 0$, and so we can write[5] $\lambda = -k^2$. The $k = 0$ mode must be trivial to satisfy the boundary conditions, so we consider only $k > 0$.

Having determined the sign of our constant of separation, our equations of motion become

$$\bar{A}^2\gamma'' + 2\bar{A}\gamma' + k^2\bar{A}^2\gamma = 0, \tag{67a}$$

$$t^2\partial_t^2\sigma + \left(k^2t^2 - 2\right)\sigma = 0. \tag{67b}$$

The general solutions to these ODEs can be expressed most simply in terms of spherical Bessel functions as

$$\gamma_k(\bar{A}) = C_1 j_0(k\bar{A}) + C_2 y_0(k\bar{A}) \tag{68a}$$

$$\sigma_k(t) = kt[C_3 j_1(kt) + C_4 y_1(kt)], \tag{68b}$$

where j_n and y_n are spherical Bessel functions of the first and second kind, respectively. The boundary condition at $\bar{A} = 0$ requires $C_2 = 0$, leading to the expected spherical Bessel function solutions for γ. If one is working with $\bar{A}_{\rm max} = \infty$, the full solution for δ_ρ is then

$$\delta_\rho(t, \bar{A}) = t\int_0^\infty dk\, kj_0(k\bar{A})[B(k)j_1(kt) + C(k)y_1(kt)] \tag{69}$$

for arbitrary functions $B(k)$ and $C(k)$. While this is useful for analytic work, it is also helpful to work with finite $\bar{A}_{\rm max}$ for numerical work, in which case we have

$$\delta_\rho(t, \bar{A}) = t\sum_n k_n j_0(k_n\bar{A})[B_n j_1(k_n t) + C_n y_1(k_n t)] \tag{70}$$

for arbitrary constants B_n and C_n, where the outer boundary creates a discrete spectrum of allowed k:

$$j_0(k\bar{A}_{\rm max}) = 0 \quad \to \quad k_n = \frac{n\pi}{\bar{A}_{\rm max}},\ n = 1, 2, 3, \ldots \tag{71}$$

In the following, we work with the discrete version, although generalizations to the continuous version are straightforward.

Given initial data for δ_ρ and $\partial_\xi\delta_\rho$, we now construct the coefficients B_n and C_n. Assuming that we are given $\delta_\rho(\xi = 0, \bar{A})$ and $\partial_\xi\delta_\rho(\xi = 0, \bar{A})$, we decompose these functions as

$$\delta_\rho(\xi = 0, \bar{A}) = \sum_n b_n j_0(k_n\bar{A}), \tag{72a}$$

$$\partial_\xi\delta_\rho(\xi = 0, \bar{A}) = \sum_n c_n j_0(k_n\bar{A}). \tag{72b}$$

We now exploit the following orthogonality relationship:

$$\int_0^1 dx\, x^2 j_0(xn\pi)j_0(xm\pi) = \frac{\delta_{nm}}{2n^2\pi^2}. \tag{73}$$

Combining Eqs. (72) and (73), we determine the coefficients b_n and c_n as

$$b_n = \frac{2k_n^2}{\bar{A}_{\rm max}}\int_0^{\bar{A}_{\rm max}} d\bar{A}\, \bar{A}^2 j_0(k_n\bar{A})\delta_\rho(\xi = 0, \bar{A}), \tag{74a}$$

$$c_n = \frac{2k_n^2}{\bar{A}_{\rm max}}\int_0^{\bar{A}_{\rm max}} d\bar{A}\, \bar{A}^2 j_0(k_n\bar{A})\partial_\xi\delta_\rho(\xi = 0, \bar{A}). \tag{74b}$$

By comparing the mode expansion (70) to Eqs. (72), we can compute B_N and C_N from b_n and c_n.

$$B_n = -b_n\cos\left(\frac{k_n}{\sqrt{3}}\right) - (b_n + 2c_n)y_1\left(\frac{k_n}{\sqrt{3}}\right) \tag{75a}$$

$$C_n = -b_n\sin\left(\frac{k_n}{\sqrt{3}}\right) + (b_n + 2c_n)j_1\left(\frac{k_n}{\sqrt{3}}\right) \tag{75b}$$

With Eq. (70) in hand, along with a method to obtain the various mode coefficients, we can now compute the related perturbed quantities. The simplest is δ_ϕ, which is trivially given by

$$\delta_\phi = -\frac{1}{4}\delta_\rho. \tag{76}$$

To obtain δ_m, we write

$$\delta_\rho = \left(1 + \frac{\bar{A}}{3}\partial_{\bar{A}}\right)\delta_m = \frac{1}{3\bar{A}^2}\partial_{\bar{A}}\left(\bar{A}^3\delta_m\right), \tag{77}$$

[5] This conclusion can also be arrived at by noting that the equation of motion is $\nabla^2\gamma = \lambda\gamma$ in spherical polar coordinates, and recalling that $-\nabla^2$ is Hermitian with appropriate boundary conditions, leading to non-negative eigenvalues.

which inverts to give

$$\delta_m = \frac{3}{\bar{A}^3}\int_0^{\bar{A}} \bar{A}^2\delta_\rho(\bar{A})d\bar{A}, \tag{78}$$

where we have used the boundary condition $\delta_m(0) = \delta_\rho(0)$ to fix the limits of integration. Noting that

$$\frac{1}{\bar{A}^3}\int_0^{\bar{A}} \bar{A}^2 j_0(k\bar{A})d\bar{A} = \frac{j_1(k\bar{A})}{k\bar{A}}, \tag{79}$$

we thus obtain

$$\delta_m(t,\bar{A}) = \frac{3t}{\bar{A}}\sum_n j_1(k_n\bar{A})[B_n j_1(k_n t) + C_n y_1(k_n t)]. \tag{80}$$

For δ_U, we use

$$\delta_U = \frac{1}{4}(\delta_m - t\partial_t\delta_m) = -\frac{1}{4}t^2\partial_t\frac{\delta_m}{t} \tag{81}$$

which follows from Eq. (57d). This gives us

$$\delta_U(t,\bar{A}) = -\frac{3t}{4\bar{A}}\sum_n j_1(k_n\bar{A})[B_n(\sin(k_n t) - 2j_1(k_n t)) - C_n(\cos(k_n t) + 2y_1(k_n t))]. \tag{82}$$

In order to compute δ_R, we need to integrate the evolution equation

$$\partial_t\delta_R = \frac{1}{t}\left(\delta_U - \frac{1}{4}\delta_\rho\right). \tag{83}$$

We integrate this from $t = 1/\sqrt{3}$ (corresponding to $\xi = 0$) to t to obtain

$$\delta_R(t,\bar{A}) = \delta_R(\xi = 0,\bar{A}) + \frac{1}{4}\sum_n \Big(B_n[\delta_{RB,n}(t,\bar{A}) - \delta_{RB,n}(1/\sqrt{3},\bar{A})] + C_n[\delta_{RC,n}(t,\bar{A}) - \delta_{RC,n}(1/\sqrt{3},\bar{A})]\Big) \tag{84}$$

where $\delta_R(\xi = 0,\bar{A})$ provides the initial conditions, and we define

$$\delta_{RB,n} = j_0(k_n\bar{A})j_0(k_n t) - 3\frac{j_1(k_n\bar{A})}{k_n\bar{A}}[j_0(k_n t) + k_n t j_1(k_n t)] \tag{85a}$$

$$\delta_{RC,n} = j_0(k_n\bar{A})y_0(k_n t) - 3\frac{j_1(k_n\bar{A})}{k_n\bar{A}}[y_0(k_n t) + k_n t y_1(k_n t)]. \tag{85b}$$

While the entire linear evolution can now be computed from an initial δ_ρ and $\partial_\xi\delta_\rho$, we do expect there to be a growing mode and a decaying mode. Looking at the density perturbation, we have modes that evolve as $ktj_1(kt)$ and $kty_1(kt)$. For $kt \ll 1$, these behave as

$$ktj_1(kt) \sim \frac{k^2t^2}{3} + O((kt)^3), \tag{86}$$

$$kty_1(kt) \sim -\frac{1}{kt} + O(kt). \tag{87}$$

The j_1 mode grows, while the y_1 mode decays. Looking beyond the leading order behavior, $xj_1(x)$ grows until $x \sim 3$, after which it oscillates. Conversely, $xy_1(x)$ decays until $x \sim 2$, after which it oscillates. It is commonly said that the growing mode oscillates once it "enters the horizon". For our time evolution, the first turnover in the growing mode occurs when the wavelength is 2/3 of the horizon scale. Note that during the growing phase, the growing mode grows as $t^2 \sim e^\xi$ independently of k (this is the rate that was found in [46]). Hence, once the decaying mode vanishes, all super-horizon modes grow at the same rate.

We can straightforwardly compute the time at which a given mode stops growing and begins oscillating. As a numerical simulation will have a maximum wavelength due to the finite domain size, there will be a time at which the last mode peaks. If the evolution remains linear at this point, it is safe to say that a black hole will not form. Hence, we can use this as a cutoff time for our evolutions. This longest wavelength mode has the minimum k, given by

$$k_1 = \frac{\pi}{\bar{A}_{\max}}. \tag{88}$$

The time when the amplitude of this mode is maximized is at the first peak of $k_1 t j_1(k_1 t)$.

$$t_{\max} \approx \frac{2.744}{k_1} \approx 0.873\bar{A}_{\max} \tag{89}$$

Replacing t with $e^{\xi/2}/\sqrt{3}$, we find

$$\xi_{\max} = 2\log(\sqrt{3}t_{\max}) \approx 0.827 + 2\log(\bar{A}_{\max}). \tag{90}$$

By this time, all growth has finished. We don't recommend evolving long past this time, as boundary artifacts will start to become significant.

B. Outer Boundary Conditions

Let us now consider a situation where we wish to investigate gravitational collapse near the origin, and desire to smoothly connect to an FRW evolution at some radius. Suppose that our region of interest is $A < A_{\max}$ on the initial time slice. By investigation of the Misner-Sharp equations, we see that it is insufficient for the local quantities U and ρ to be equal to their FRW values for $A \geq A_{\max}$ to ensure FRW evolution, as an incorrect mass

inside the radius $A_{\max}$ will then cause the evolution to differ from FRW. Thus, in order to ensure FRW evolution for $A \geq A_{\max}$, we must also require $m(A_{\max}) = m_b(A_{\max})$. This matching condition implies that any overdensity must be surrounded by a corresponding underdensity in order to smoothly connect to FRW.

We can translate this into a condition on $\tilde{m}$. If $m(A_{\max}) = m_b(A_{\max})$, we have

$$0 = \int_0^{A_{\max}} R^2 \partial_A R(\rho - \rho_b) dA \,. \tag{91}$$

Writing $\rho = \rho_b(1 + \delta_\rho)$, this becomes

$$0 = \int_0^{A_{\max}} R^2 \partial_A R \delta_\rho dA \,. \tag{92}$$ eq:deltamcond

We now use Eq. (44d) to write

$$\delta_\rho = \frac{1}{3\tilde{R}^2 \partial_A \tilde{R}} \partial_A (\tilde{R}^3 \delta_m) \tag{93}$$

without approximation. Combining the previous two equations and using $R = a R_H \tilde{R}$ yields

$$0 = \int_0^{A_{\max}} \partial_A (\tilde{R}^3 \delta_m) dA = \tilde{R}^3 \delta_m \Big|_{A_{\max}} \,. \tag{94}$$

Hence, we see that matching to FRW requires $\delta_m = 0$ or $\tilde{m} = 1$ for $A \geq A_{\max}$. We can also take the limit as $A_{\max} \to \infty$ such that the matching happens asymptotically, which requires

$$\lim_{A \to \infty} \tilde{R}^3 \delta_m = 0 \,. \tag{95}$$ eq:limit

This extends the linearized argument given by Polnarev and Musco [46]. It is important to note that this condition is not guaranteed to be preserved under time evolution due to waves traveling outside the domain, as we now discuss.

For the purposes of matching to FRW numerically, it is helpful to have the initial data approach the background values at the boundary of the computational domain. However, as the evolution equations depend on derivatives of the local variables, data that matches to FRW at the boundary at one time is not guaranteed to match at a later time. In particular, a central perturbed region tends to gradually expand out, particularly when it doesn't form a black hole.

This means that a physical boundary condition at the outer boundary of the computational domain doesn't exist. However, in order to solve the equations, an outer boundary needs to be specified, as there are two characteristics to the equations of motion, one traveling inwards and one traveling outwards. Without a boundary condition, no control over the ingoing characteristic is exercised, and the evolution rapidly becomes unstable. Just like a one-dimensional wave equation on a finite domain, a single boundary condition is required at the outer boundary.

A number of works in the literature have employed the Dirichlet boundary condition $\rho(A_{\max}) = \rho_b$. This boundary condition does an excellent job of maintaining stability at the outer boundary, but is unphysical in that it asserts that what is outside the boundary remains FRW for all time, contrary to the argument given above. As such, it creates a reflecting boundary condition where outgoing waves reflect negatively off the outer boundary. We experimented with a Neumann boundary condition $\tilde{\rho}' = 0$ at the boundary, finding that waves were reflected positively, as expected.

One way in which to ameliorate this issue is to begin the evolution with a sufficiently large domain such that traveling waves do not reach the boundary before it can be determined whether a black hole has formed/will not form. However, this is computationally expensive. One solution to this, advocated by Nakama *et al.* [49], is to begin with a reasonably small domain that matches to FRW on the boundary, and watch for the boundary to deviate from FRW by a small quantity. Then, expand the domain by appending FRW values to the edge of the domain, and watch the new boundary for deviations. This would seem to work well, except for the fact that they required pinning ρ at the boundary to its FRW value, and watching U deviate, whereas in principle, both should be allowed to vary. In a similar vein, Hawke and Stewart [42] suggested adding extra gridpoints at the boundary of the domain as the evolution proceeds. None of these approaches are appealing to us.

We therefore desire a boundary condition on the outer boundary that allows waves to travel through the boundary with minimal reflection. To do so, we construct linear solutions which behave like traveling waves and find a condition which forbids incoming waves. Since we are constructing traveling waves, we will need to disregard our earlier boundary conditions for the origin and the outside. This allows the use of the y_1 modes in creating the traveling waves.

For our boundary condition, we seek a linear constraint on $\partial_\xi \delta_u$ of the form

$$\partial_\xi \delta_U = W \delta_u' + X \delta_u + Y \delta_m' + Z \delta_m \tag{96}$$ eq:boundary_form

that is satisfied for all time ξ at the outer boundary $A_{\max}$ by only the outward traveling waves. We thus desire to know the form of the waves in terms of δ_m. Constructing complex waves to make the wave-like nature obvious, the desired modes are

$$\begin{aligned} \delta_m^{\text{in}} &= \frac{t}{\bar{A}} \big(j_1(k\bar{A}) \pm i y_1(k\bar{A})\big)\big(j_1(kt) \pm i y_1(kt)\big) \\ &= \frac{1}{k^4 \bar{A}^3 t} e^{\pm ik(\bar{A}+t)} (k\bar{A} \pm i)(kt \pm i) \qquad (97a) \\ \delta_m^{\text{out}} &= \frac{t}{\bar{A}} \big(j_1(k\bar{A}) \pm i y_1(k\bar{A})\big)\big(j_1(kt) \mp i y_1(kt)\big) \\ &= \frac{1}{k^4 \bar{A}^3 t} e^{\pm ik(\bar{A}-t)} (k\bar{A} \pm i)(kt \mp i) \,. \qquad (97b) \end{aligned}$$

These form a complete basis for the modes of δ_m. At large $\bar{A}$ and large t, $\delta_m^{\text{out}} \approx \frac{1}{k^2 \bar{A}^2} e^{\pm ik(\bar{A}-t)}$, which is a radially

outward traveling wave with amplitude that decays as $\bar{A}^{-2}$. This decay is exactly what is expected from the wave spreading out spherically as the radius grows. Similarly, at large $\bar{A}$ and t, $\delta_m^{\rm in} \approx \frac{1}{k^2\bar{A}^2} e^{\pm ik(\bar{A}+t)}$ describes an inward traveling wave.

To obtain the desired boundary condition, we first write $\delta_m^{\rm out}$ in terms of ξ:

$$\delta_m^{\rm out} = \frac{e^{\pm i\left(\bar{A}-e^{\xi/2}/\sqrt{3}\right)k-\frac{\xi}{2}}}{\bar{A}^3k^4}(\bar{A}k\pm i)\left(\frac{e^{\xi/2}}{\sqrt{3}}k\mp i\right). \quad \texttt{eq:mout} \tag{98}$$

We then use Eq. (57d) to construct $\delta_U^{\rm out} = \frac{1}{4}\delta_m^{\rm out} - \frac{1}{2}\partial_\xi\delta_m^{\rm out}$.

$$\delta_U^{\rm out} = \frac{e^{\pm i\left(\bar{A}-e^{\xi/2}/\sqrt{3}\right)k-\frac{\xi}{2}}}{\bar{A}^3k^4}(\bar{A}k\pm i)\left(\frac{2e^{\xi/2}}{\sqrt{3}}k\pm i\frac{e^{\xi}}{3}k^2\mp 2i\right). \quad \texttt{eq:uout} \tag{99}$$

There is a unique set of $\{W, X, Y, Z\}$ that solves Eq. (96) with Eqs. (98) and (99) for all k, $\bar{A}$ and ξ:

$$W = -\frac{e^{\xi/2}}{2\sqrt{3}} \tag{100a}$$

$$X = -\sqrt{3}\frac{\bar{A}^2+\sqrt{3}\bar{A}e^{\xi/2}+e^{\xi}}{2\bar{A}(\sqrt{3}\bar{A}+e^{\xi/2})} \tag{100b}$$

$$Y = e^{\xi/2}\frac{6\bar{A}^2+2\sqrt{3}\bar{A}e^{\xi/2}+e^{\xi}}{24\bar{A}(\sqrt{3}\bar{A}+e^{\xi/2}} \tag{100c}$$

$$Z = e^{\xi/2}\frac{4\bar{A}^2+2\sqrt{3}\bar{A}e^{\xi/2}+e^{\xi}}{8\bar{A}^2(\sqrt{3}\bar{A}+e^{\xi/2})}\,. \tag{100d}$$

These expressions can also be rewritten replacing ξ with the speed of sound, $c_s = \frac{e^{\xi/2}}{\sqrt{12}}$:

$$W = -c_s \tag{101a}$$

$$X = -\frac{12c_s^2+6c_s\bar{A}+\bar{A}^2}{2\bar{A}(2c_s+\bar{A})} \tag{101b}$$

$$Y = \frac{c_s(2c_s^2+2c_s\bar{A}+\bar{A}^2)}{2\bar{A}(2c_s+\bar{A})} \tag{101c}$$

$$Z = \frac{c_s(3c_s^2+3c_s\bar{A}+\bar{A}^2)}{\bar{A}^2(2c_s+\bar{A})}. \tag{101d}$$

As our nonlinear evolution is in the variables $\tilde{U}$ and $\tilde{m}$, we need to transform this boundary condition using the definitions of the linear variables (54). Additionally, we replace $\bar{A}$ by $\tilde{R}$ and divide derivatives with respect to $\bar{A}$ by $\tilde{R}'$ to construct a boundary condition which is invariant under reparameterizations of $\bar{A}$.

$$\partial_\xi\tilde{U} = -X\tilde{R} + Z\tilde{R}(\tilde{m}-1) + (X-\frac{W}{\tilde{R}})\tilde{U} + Y\tilde{R}\frac{\tilde{m}'}{\tilde{R}'} + W\frac{\tilde{U}'}{\tilde{R}'} + \frac{\tilde{U}\partial_\xi\tilde{R}}{\tilde{R}}\,. \tag{102}$$

Having a minimally reflecting boundary helps with the numerical evolution in a number of ways. It allows waves to escape the computational domain, which in turn allows us to reduce our domain size without affecting the evolution. This significantly increases the computational speed of our evolutions. We find that our boundary condition works remarkably well, as we show in Fig. 1.

One caveat to the use of this boundary condition is that it was computed using linear perturbation theory. As such, if a wave with nonlinear amplitude hits the boundary, the boundary condition doesn't work nearly so well (although it works significantly better than the reflecting boundary conditions). Something else to note is that artificial viscosity should be turned off for gridpoints near the boundary, as the boundary condition doesn't account for it at all.

C. Constraints on Initial Data

There are a number of constraints on initial data, arising from both physical and desirable considerations. Here, we construct the various constraints, and then apply them to the solutions found above. We assume that initial data is specified in terms of $\tilde{m}$, $\tilde{R}$ and $\tilde{U}$.

1. *Physical Constraints*

The most basic physical constraint is that $\tilde{m}$ and $\tilde{R}$ are positive, as neither m nor R can become negative. As U can be negative, so may $\tilde{U}$. By spherical symmetry, $\tilde{m}$ is an even function, and so must have zero derivative at the origin.

Next, we require both R and m to be monotonically increasing with $\bar{A}$. These yield the constraints

$$0 < \tilde{R}' \quad \texttt{eq:condition1} \tag{103}$$

$$0 \le \tilde{m} + \frac{\tilde{R}}{3\tilde{R}'}\tilde{m}' \equiv \tilde{\rho} \tag{104}$$

respectively. Requiring the metric component g_{AA} to be positive for the initial data requires that $\bar{\Gamma}^2 \ge 0$. This constraint can be written as

$$\tilde{R}^2\tilde{m} - \tilde{U}^2 \le 1\,. \quad \texttt{eq:newgammacond} \tag{105}$$

Writing this condition in terms of linearized variables yields

$$\delta_m - 2\delta_U \le \frac{1}{\bar{A}^2}\,, \quad \texttt{eq:linearizedgammaconst} \tag{106}$$

which places a stringent constraint on δ_m and δ_U at large $\bar{A}$ beyond simply requiring them to be perturbative.

2. *Desirable Constraints*

In addition to the physical constraints described above, there are a few desirable constraints also. The first is a nu-

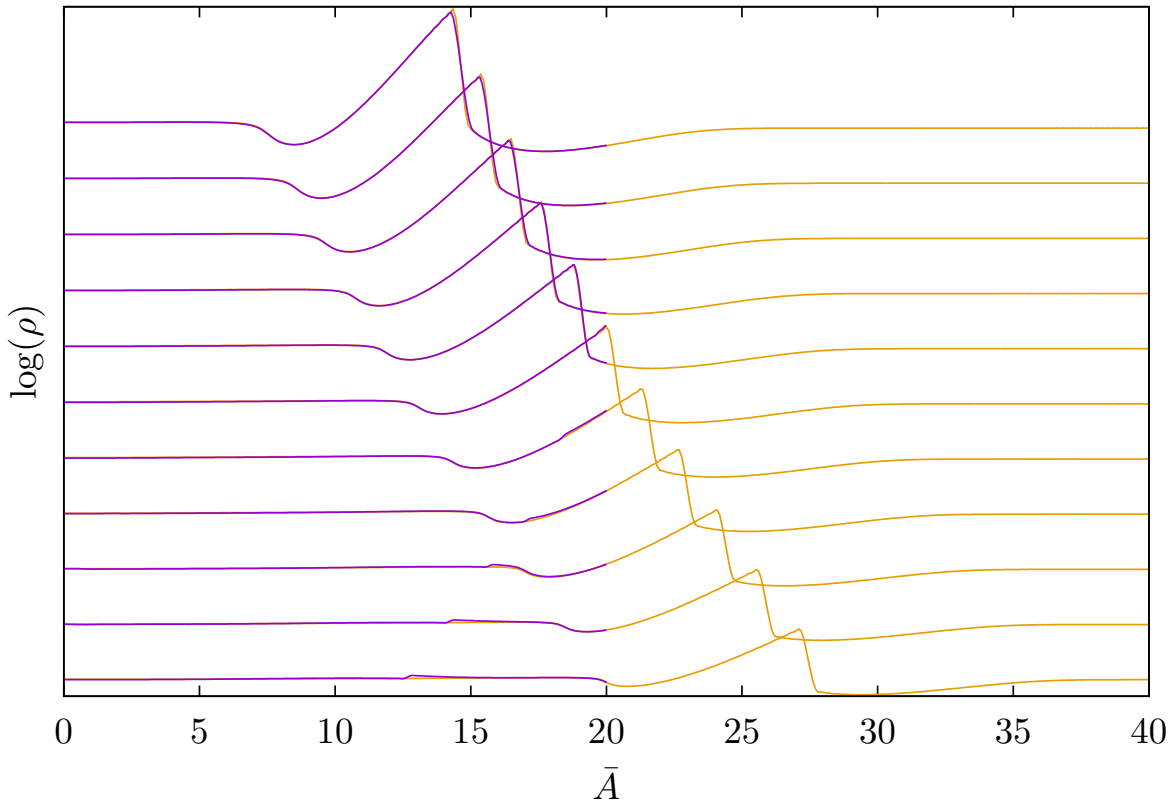

Figure 1. Demonstration of our boundary condition. This plots density as a function of comoving radius at various times. The top curve is the earliest curve in this set, and the bottom curve is the latest. The curve in purple has an outer boundary at $\bar{A} = 20$, while the curve in teal has an outer boundary at $\bar{A} = 40$. The y axis is logarithmic, but the overall scaling is unimportant; it was chosen this way simply to show data at different timesteps clearly.

This run did not form a black hole, but instead sent a wave of material propagating outwards. We see that our boundary condition allows the purple curve to track the teal curve remarkably well, despite terminating halfway along the domain. The largest deviations occur in the bottom two curves, which show that there was a small reflected component at the boundary. As the characteristics evolve as $\sim 1/\bar{A}$, even a very small reflected component grows as it moves towards the origin. **FIXME: REWRITE CAPTION**

merical issue: it is recommended that initial data connect smoothly to FRW at the boundary of the computational domain. This improves the accuracy of the evolution by reducing unphysical reflections from the boundary.

The second desirable constraint, as discussed previously, is that the initial data should consist of a growing mode only[6]. If we are given initial data for $\delta_\rho(\xi = 0, \bar{A})$ only, we can construct the initial data for $\partial_\xi \delta_\rho(\xi = 0, \bar{A})$ such that the initial conditions contain no decaying mode. The b_n coefficients can be computed from Eq. (74a), while the c_n coefficients can be computed from Eq. (75b) by requiring that[7] $C_n = 0$:

$$c_n = \frac{b_n}{2}\left(\frac{\sin(k_n/\sqrt{3})}{j_1(k_n/\sqrt{3})} - 1\right). \tag{107}$$

This gives

$$B_n = \frac{b_n}{(k_n/\sqrt{3}) j_1(k_n/\sqrt{3})}. \tag{108}$$

It is curious that the denominator can go to zero here when $k_n/\sqrt{3}$ is a root of j_1. Note that if $j_1(k_n/\sqrt{3}) = 0$, the corresponding mode is

$$\delta_\rho(t, \bar{A}) = B_n\, k_n t\, j_0(k_n \bar{A}) j_1(k_n t)\,, \tag{109}$$

[6] It is not imperative that the decaying mode is nonexistent in initial data; so long as the evolution starts with the perturbation sufficiently far outside the cosmological horizon, the decaying mode will have time to decay before the perturbation enters the horizon.

[7] Note that this will also kill the decaying mode for sub-horizon modes, which no longer decay, but only oscillate; this should not be a problem for initial data with essentially no power on subhorizon scales.

which vanishes when evaluated at $t = 1/\sqrt{3}$. It is thus not surprising that we cannot compute B_n for this mode, as δ_ρ contains no information about it! Note that this denominator can only vanish if $j_1(k_n t)$ has completed its first oscillation, so this divergence only occurs for modes that are subhorizon, when the decaying mode doesn't necessarily need to vanish.

When C_n is vanishing we can write δ_m and δ_U as follows:

$$\delta_m(t,\bar{A}) = \frac{3}{\bar{A}}\sum_n j_1(k_n\bar{A})\frac{B_n}{k_n}(k_n t)j_1(k_n t) \tag{110}$$

$$\delta_U(t,\bar{A}) = -\frac{3}{4\bar{A}}\sum_n j_1(k_n\bar{A})\frac{B_n}{k_n}(k_n t)(\sin(k_n t) - 2j_1(k_n t))\,. \tag{111}$$

Looking at superhorizon modes only, we can expand these expressions for small $k_n t$, finding

$$k_n t\, j_1(k_n t) \approx k_n t\,(\sin(k_n t) - 2j_1(k_n t)) \approx \frac{(k_n t)^2}{3}\,. \tag{112}$$

Hence, we can write

$$\delta_m(t,\bar{A}) \approx -4\delta_U(t,\bar{A}) \approx \frac{t^2}{\bar{A}}\sum_n j_1(k_n\bar{A})B_n k_n\,. \tag{113}$$

This relationship between δ_m and δ_U for growing superhorizon modes has been used by other authors to construct initial data. Note that the constraint (106) then becomes

$$\delta_m \leq \frac{2}{3\bar{A}^2}\,, \tag{114}$$

giving a stringent upper bound on δ_m at large radii.

The other desirable constraint in initial data is perturbative initial conditions. While we cannot construct a constraint on individual B_n and C_n coefficients, it is straightforward to check the initial data to ensure that δ_ρ, δ_U, δ_R and δ_m remain perturbative.

D. Relation to the Literature

We now relate our results to other works in the literature.

1. Density and Mass Relationships

We begin by writing the relationship between $\tilde{\rho}$ and $\tilde{m}$ in various ways. The exact relationship is given by Eq. (44d), and can also be written as

$$\tilde{\rho} = \frac{(\tilde{R}^3\tilde{m})'}{(\tilde{R}^3)'}\,. \tag{115}$$

Using the result (95), this can be integrated to give

$$\tilde{m}(\bar{A}) = 1 + \frac{1}{\tilde{R}^3(\bar{A})}\int_\infty^{\bar{A}} (\tilde{R}^3(\bar{A}'))'\delta_\rho(\bar{A}')\,d\bar{A}' \tag{116}$$

where $\delta_\rho = \tilde{\rho} - 1$ is just the usual cosmological density contrast. The linearized version of these two relationships are

$$\delta_\rho = \frac{(\bar{A}^3\delta_m)'}{3\bar{A}^2} = \delta_m + \frac{\bar{A}}{3}\delta_m' \tag{117}$$

$$\delta_m = \frac{3}{\bar{A}^3}\int_\infty^{\bar{A}} \bar{A}'^2\delta_\rho(\bar{A}')\,d\bar{A}' \tag{118}$$

with $\delta_m = \tilde{m} - 1$. It is curious that these formulas for δ_m and $\tilde{m}$ are written as integrals from infinity inwards, whereas m was initially defined as an integral from the origin outwards. The reason for this equivalence is that we are assuming a matching to FRW at infinity.

2. Fractional Mass Excess

A number of papers compute the fractional mass excess inside the cosmological horizon, denoted by the (much-overworked) symbol δ. This quantity has been computed in different ways, with variations based on gauge and a choice on how the background mass is quantified. Carr's original formulation [14, 15] used a uniform Hubble constant gauge with two shells of unequal density. A more recent approach by Harada *et al.* [54] revisited Carr's approach. Furthermore, they conveniently represented their result in the gauge we have employed.

The fractional mass excess associated with a perturbation is computed when the perturbation enters the horizon. In our language, the horizon has proper radius $R = 1/H = R_H e^\xi$, corresponding to $\tilde{R}(\bar{A}_H) = e^{(1-\alpha)\xi}$. The perturbation is said to enter the horizon when the density at the horizon is equal to the FRW density (followed by a sub-FRW underdensity to compensate for the overdensity inside the horizon). The time of horizon crossing is a gauge-dependent quantity, but within a given gauge, it is well-defined.

The fractional mass excess δ is then defined by

$$\delta = \frac{m(\bar{A}_H)}{m_b(\bar{A}_H)} - 1 \tag{119}$$

at this time, where $m_b(\bar{A}_H)$ is given by[8]

$$m_b(\bar{A}_H) = \frac{4\pi}{3}R^3(\bar{A}_H)\rho_b\,. \tag{120}$$

[8] Note that some authors choose to use R_b instead of R in this expression.

In our language, the fractional mass excess is simply given by

$$\delta = \tilde{m}(\bar{A}_H) - 1 = \delta_m(\bar{A}_H)\,, \tag{121}$$

evaluated at the time of horizon crossing.

It is possible to estimate the fractional mass excess from initial data by identifying the radius of the perturbation and assuming superhorizon linear growth until horizon reentry (see Polnarev and Musco [46]). However, this assumes that modes that enter the horizon continue to grow, leading to a biased result. In order to extract the fractional mass excess from a numerical run, one should monitor the density $\tilde{\rho}$ at the horizon. When it drops beneath one, read off $\delta = \tilde{m} - 1$ at that point in space and time.

Harada *et al.* [54] calculated that black holes are likely to form for $\delta > \delta_c$ with

$$\delta_c = \frac{3(1+w)}{5+3w} \sin^2\left(\frac{\pi\sqrt{w}}{1+3w}\right)\,. \tag{122}$$

This result is given in the gauge we employ here. For $w = 1/3$, this yields $\delta_c \approx 0.4135$.

Using the fractional mass excess as an indicator of whether or not a black hole will form has some obvious deficiencies: if the density profile is such that the density contrast becomes negative briefly before becoming positive again, this method will not capture the appropriate overdensity. Similarly, a long tail of a positive density contrast can also lead to erroneous results. In general, the dependence of black hole formation on the details of the density profile are not particularly well captured by the estimate in Eq. (122), although it works reasonably well as a rule of thumb. This is to be expected, as Harada *et al.* were more interested in correctly estimating the dependence of δ_c on the equation of state than the initial profile. In order to overcome some of these deficiencies, Nakama *et al.* [49] and Musco [55] have begun exploring more appropriate quantities for identifying black hole formation based on the density profile.

3. Curvature Perturbation

An approach to generating appropriate initial conditions based on curvature perturbations has been championed by Polnarev [46, 47, 49]. This approach is based around the fact that

$$\Gamma^2 = 1 - KA^2 \tag{123}$$

for a curved FRW universe. Accordingly, Polnarev and Musco [46] suggested letting

$$\Gamma^2 = 1 - K(t, A)A^2 \tag{124}$$

and describing the dynamics of the curvature perturbation $K(t, A)$. It was claimed that this picks out the growing mode; indeed, the growing mode is the particular solution of an ODE driven by the existence of the curvature perturbation. The decaying mode exists as the homogeneous solution of the equation, which was neglected entirely.

The method utilizes a time-dependent small parameter ϵ^2 where

$$\epsilon = \frac{1}{\dot{a}^2 r_0^2} \tag{125}$$

for some arbitrary, initially super-horizon comoving scale r_0. It is useful to note that

$$\epsilon = \frac{t_0^2}{\alpha^2 r_0^2} e^{2(1-\alpha)\xi}\,. \tag{126}$$

Eventually, the various quantities δ^1_X are related to $K(t_0, A)$ at first order in perturbations. The relationship between K and our variables comes from matching Eqs. (44f) and (124).

$$K(\xi, \bar{A}) = \frac{1}{R_H^2} e^{2(\alpha-1)\xi} \tilde{R}^2 \left(\tilde{m} - \tilde{U}^2\right) \tag{127}$$

Substituting $\tilde{m}$, $\tilde{U}$ and $\tilde{R}$ to linear order, we obtain

$$K(\xi, \bar{A}) = \frac{1}{R_H^2} \left(\delta_m - 2\delta_U\right)\,. \tag{128}$$

There are two ways to use K. The first is just to use it as a method to construct initial data. However, because of various approximations, when the actual curvature perturbation is computed from initial data constructed using K, it doesn't return exactly K. The second approach is to use K as an evolution variable to replace U. The issue with this approach is that K is related to U^2 instead of U, and as such is ambiguous whenever U may be negative. We find our variables of evolution somewhat cleaner (particularly in not requiring a dimensionful scale r_0), and note that one can always compute K from Γ^2 if desired.

4. Bardeen Gauge Invariant Variables

In order to connect to cosmological perturbation theory, it is useful to find the relation between our variables and the Bardeen gauge invariant variables [56]. As the Bardeen variables are gauge invariant at linear order, here we work with our linearized variables also. The relevant relationships are derived in Appendix B, and reproduced here for convenience[9].

$$\Phi = \Psi = -\frac{1}{2} e^{2(\alpha-1)\xi} \int_{\bar{A}}^{\infty} \bar{A}'\, \delta_m(\bar{A}') d\bar{A}' \tag{130}$$

---

[9] The quantities Φ and Ψ correspond to the Newtonian gauge metric

$$ds^2 = -(1+2\Phi)dt^2 + a^2(1-2\Psi)dx^2\,. \tag{129}$$

As δ_m grows as $t^2 \sim e^{2(1-\alpha)\xi}$ in the superhorizon linear regime, we see that Φ and Ψ are constant in this description, as we expect. We also find that the Bardeen variables are equal, as expected for a perfect fluid with no anisotropic shear stress.

To get a grasp of the behavior of Φ and Ψ, using $\delta_\rho = \delta_m + \bar{A}\delta_m'/3$ and integration by parts, we can write

$$\int_{\bar{A}}^{\infty} \bar{A}'\delta_m(\bar{A}')d\bar{A}' = \bar{A}^2\delta_m - 3\int_{\bar{A}}^{\infty} \bar{A}'\delta_\rho(\bar{A}')d\bar{A}' \quad (131)$$

where the limit $\bar{A}^2\delta_m \to 0$ as $\bar{A} \to \infty$ by Eq. (95) and the squeeze theorem. Using this, we have

$$\Phi = \frac{1}{2}e^{2(\alpha-1)\xi}\left(-\bar{A}^2\delta_m + 3\int_{\bar{A}}^{\infty} \bar{A}'\,\delta_\rho(\bar{A}')d\bar{A}'\right). \quad (132)$$

Generally speaking, when δ_m is large and positive, the second term will be subdominant. To see this, consider some $\bar{A}$ beyond which $\delta_\rho \le 0$. Then

$$\bar{A}^2\delta_m = \frac{3}{\bar{A}}\int_{\bar{A}}^{\infty} \bar{A}^2(-\delta_\rho)d\bar{A} > 3\int_{\bar{A}}^{\infty} \bar{A}(-\delta_\rho)d\bar{A} \quad (133)$$

where the equality comes from integrating Eq. (117). Thus, we can write

$$\Phi,\, \Psi \simeq -\frac{1}{2}\bar{A}^2\delta_m\,. \quad (134)$$

While this appears to grow as $\bar{A}^2$, recall that δ_m is subject to the constraint (114) and hence must decay like $1/\bar{A}^2$, giving reasonable values for Φ and Ψ.

We now look at translating quantities in the opposite direction. Let us assume that at the end of inflation, we are given the gauge invariant metric perturbation Ψ or Φ, the gauge invariant velocity perturbation V, and the gauge invariant density perturbation Δ (see Appendix B). We have

$$\delta_m = \frac{2}{\bar{A}}\Phi' e^{2(1-\alpha)\xi} \quad (135a)$$

$$\delta_U = \frac{V'}{R_H\bar{A}}e^{(1-\alpha)\xi} \quad (135b)$$

$$\delta_\rho = \Delta\,, \quad (135c)$$

eq:Delta

where primes again refer to derivatives with respect to $\bar{A}$. Once δ_U and δ_ρ are known, $\partial_\xi\delta_\rho$ can be computed using Eq. (57c), and from there, one can compute the full linear evolution. Also note that δ_m and δ_ρ can each be obtained from the other. We should also point out that these formulas require Φ', $V' \to 0$ sufficiently rapidly as $\bar{A} \to 0$ (this is a requirement of spherical symmetry).

We can also construct the gauge invariant variables in terms of the mode coefficients B_n and C_n from above. Working with $w = 1/3$ and writing in terms of $t = \exp(\xi/2)/\sqrt{3}$, we have

$$\Phi = \Psi = -\frac{1}{2t}\sum_n \frac{j_0(k_n\bar{A})}{k_n}[B_n j_1(k_n t) + C_n y_1(k_n t)] \quad (136a)$$

$$V = \frac{\sqrt{3}}{4}R_H\sum_n \frac{j_0(k_n\bar{A})}{k_n}[B_n(\sin(k_n t) - 2j_1(k_n t)) - C_n(\cos(k_n t) + 2y_1(k_n t))] \quad (136b)$$

$$\Delta = t\sum_n k_n j_0(k_n\bar{A})[B_n j_1(k_n t) + C_n y_1(k_n t)] \quad (136c)$$

Note that the last of these is equivalent to Eq. (70) as a result of Eq. (135c).

V. COSMOLOGICAL HERNANDEZ-MISNER FORMALISM

Though the Misner-Sharp formalism is very practical for the numerical study of spherically symmetric spacetimes, it breaks down once a singularity forms. When simulating the formation of a primordial black hole, this makes it difficult to calculate its final mass. In order to deal with the formation of a singularity, Hernandez and Misner developed a formalism that uses radially outward traveling light rays to define a time coordinate [37]. The idea is to define a time coordinate based on the time at which an outgoing radial light ray starting from a given event reaches a distant observer. As time runs slower in a deep gravitational well, in this coordinate system, it takes infinite coordinate time for an event horizon to form, and so a singularity never forms. This formalism has been applied to primordial black hole formation in Refs. [35, 42, 43, 45, 49], where it has typically been built upon the work of Baumgarte *et al.* [36]. Rather than derive the Hernandez-Misner formalism and then perform a messy transformation to the cosmological variables, we present a more direct derivation that skips directly to the cosmological variables. As we found that artificial viscosity was much less useful in this formalism, we leave it out of the following derivations for clarity, although it is straightforward to include if desired.

We begin by defining a new coordinate $u(t, A)$ to replace the time coordinate. The derivatives of u are given by

$$du = \left.\frac{\partial u}{\partial t}\right|_A dt + \left.\frac{\partial u}{\partial A}\right|_t dA \quad (137)$$

eq:dudef

$$= e^{-\psi}(e^{\phi}dt - e^{\lambda/2}dA) \quad (138)$$

where we've demanded that the partial derivatives of u are such that du vanishes along an outgoing null geodesic, and ψ is any function that makes du a perfect differential. This coordinate system is known as "observer time coordinates", as each u corresponds to what an observer

at a large radius sees when looking towards the origin. Solving Eq. (137) for dt and substituting into the metric (4), the metric in the new coordinate system becomes

$$ds^2 = -e^{2\psi}du^2 - 2e^{\psi+\lambda/2}dudA + R^2 d\Omega^2 . \quad (139)$$ eq:HMmetric

Our approach in this new coordinate system will be to evolve $\tilde{m}$, $\tilde{U}$, $\tilde{R}$ as functions of u and $\bar{A}$. In addition to this, we need to know the old time variable ξ as a function of u and $\bar{A}$, as it appears in the equations of motion, and is no longer constant across the slice. We assume that for a given u, we know these four variables as functions of $\bar{A}$, and work to construct their evolution equations.

To transform the equations of motion to this new coordinate system, we define the following coordinate-invariant operators.

$$D_t = u^\mu \partial_\mu, \quad D_r = v^\mu \partial_\mu \quad (140)$$ eq:HMderiv

Here, $u^\mu = (e^{-\phi}, 0, 0, 0)$ is the comoving fluid four-velocity and $v^\mu = (0, e^{-\lambda/2}, 0, 0)$ in the Misner-Sharp coordinate system. Given the metric (4), we see that D_t is the derivative with respect to proper time at a fixed spatial coordinate, and D_r is the derivative with respect to proper distance at a fixed time and angle.

These derivatives can be transformed to the new coordinate system through careful application of the chain rule.

$$\left.\frac{\partial}{\partial u}\right|_A = \left.\frac{\partial t}{\partial u}\right|_A \left.\frac{\partial}{\partial t}\right|_A = e^{\psi-\phi}\partial_t \quad (141)$$

$$\left.\frac{\partial}{\partial A}\right|_u = \left.\frac{\partial t}{\partial A}\right|_u \left.\frac{\partial}{\partial t}\right|_A + \left.\frac{\partial}{\partial A}\right|_t = e^{\lambda/2-\phi}\partial_t + \partial_A|_t \quad (142)$$

Hence, we have

$$D_t = e^{-\psi}\partial_u, \qquad D_r = e^{-\lambda/2}\partial_A|_u = e^{-\psi}\partial_u . \quad (143)$$ eq:invariantderivs

We also define the operator

$$D_k \equiv D_t + D_r = e^{-\lambda/2}\partial_A|_u \quad (144)$$

as the derivative along an outgoing null ray.

A. Computing ψ

We begin by investigating the behavior of the lapse ψ. As du is a perfect differential, we may write

$$\partial_t \partial_A u = \partial_A \partial_t u . \quad (145)$$

and use the derivatives from Eq. (137) to obtain

$$D_k\psi = D_r\phi + \frac{1}{2}D_t\lambda . \quad (146)$$ eq:psi1

Using Eq. (10) in the form

$$D_r\phi = -\frac{D_r P}{\rho + P} \quad (147)$$ eq:Drphi

and Eq. (11b) in the form

$$\frac{1}{2}D_t\lambda = \frac{D_r U}{\Gamma} \quad (148)$$ eq:Dtlambda

yields

$$D_k\psi = \frac{D_r U}{\Gamma} - \frac{D_r P}{\rho + P} . \quad (149)$$ eq:workingonpsi

Next, write Eq. (17) as

$$D_t U = -\Gamma\frac{D_r P}{\rho + P} - \frac{m + 4\pi P R^3}{R^2} . \quad (150)$$

Combining this with Eq. (149) yields

$$\Gamma D_k\psi = D_k U + \frac{m}{R^2} + 4\pi R P . \quad (151)$$ eq:HMpsi

In principle, this allows us to compute ψ by integrating inwards from an outer boundary condition. However, we will shortly develop a better way to compute ψ.

First though, we show that a horizon never forms in this coordinate system. Start with Eq. (13), and apply D_k to both sides.

$$\Gamma D_k\Gamma = U D_k U - \frac{D_k m}{R} + \frac{m}{R^2}D_k R \quad (152)$$

Next, use Eqs. (9c) and (15) to find

$$D_k m = 4\pi R^2(\rho\Gamma - PU), \quad (153)$$ eq:Dkm

and note that $D_k R = U + \Gamma$. Finally, use Eq. (151) to substitute for m/R^2. When the dust settles, we obtain

$$D_k[e^{-\psi}(\Gamma + U)] = -e^{\psi}4\pi R(\rho + P). \quad (154)$$ eq:HMpsi2

Thus, in the null coordinate system, assuming $P \geq -\rho$ (no phantom equations of state), $e^{-\psi}(\Gamma + U)$ must be monotonically decreasing with increasing coordinate radius. An observer at large radius sees positive $D_k R$, and hence $\Gamma + U$ must be positive everywhere. Noting that the condition under which a trapped surface forms is

$$U + \Gamma \equiv D_k R \leq 0, \quad (155)$$

a horizon never forms. We can see how the null slicing condition avoids a black hole in Fig. 5.

Musco *et al.* [45] point out that as $D_k R$ and e^{ψ} can only reach zero together as $u \to \infty$, care must be taken in the numerical evolution equations to ensure that this synchronization occurs, else negative values of $D_k R$ may result. Instead of integrating Eq. (151) directly, it is safer to integrate Eq. (154) in the form

$$\partial_A[e^{-\psi}(\Gamma + U)] = -e^{\lambda/2-\psi}4\pi R(\rho + P) . \quad (156)$$ eq:HMpsi3

This can be written in the cosmological variables as follows.

$$\partial_{\bar{A}}[e^{-\psi}e^{(\alpha-1)\xi}(\bar{\Gamma} + \tilde{U})] = -R_H e^{\lambda/2-\psi}4\pi R\rho(1 + w) \quad (157)$$

Taking $e^{(\alpha-1)\xi}$ outside of the derivative and using Eq. (169) from below, this simplifies to

$$\partial_{\bar{A}} \ln\left(e^{-\psi}(\bar{\Gamma}+\tilde{U})\right) = \xi'\left(1-\alpha-\frac{e^{\phi}\tilde{R}\tilde{\rho}}{\bar{\Gamma}+\tilde{U}}\right) \tag{158}$$

eq:hmlapsecomputation

where $\xi' = \partial_{\bar{A}}\xi\big|_u$. This can be integrated inwards from the outer boundary, given a boundary condition on ψ which we discuss below.

B. Deriving the Equations of Motion

We now derive the cosmological equations of motion in the Hernandez-Misner coordinate system. Noting that

$$D_t = \frac{e^{-\phi-\xi}}{\alpha R_H}\partial_\xi, \quad D_r = \frac{e^{-\lambda/2}}{R_H}\partial_{\bar{A}}\big|_t, \tag{159}$$

we can write our cosmological equations of motion in terms of the invariant derivatives.

$$D_t\tilde{R} = \frac{1}{R_H}\left(e^{-\xi}\tilde{U} - e^{-\phi-\xi}\tilde{R}\right) \tag{160a}$$

$$D_t\tilde{m} = \frac{2}{\alpha R_H}e^{-\phi-\xi}\tilde{m} - \frac{3}{R_H}e^{-\xi}\frac{\tilde{U}}{\tilde{R}}\left(\tilde{P}+\tilde{m}\right) \tag{160b}$$

$$D_t\tilde{U} = -\frac{e^{-\xi}}{R_H}\left[\frac{\bar{\Gamma}^2 D_r\tilde{P}}{D_r(\tilde{R})(\tilde{\rho}+\tilde{P})} + \frac{\tilde{R}}{2}\left(\tilde{m}+3\tilde{P}\right)\right] + \frac{e^{-\phi-\xi}}{\alpha R_H}(1-\alpha)\tilde{U} \tag{160c}$$

$$\tilde{\rho} = \tilde{m} + \frac{\tilde{R}D_r\tilde{m}}{3D_r\tilde{R}} \tag{160d}$$

We don't need the equation of motion for ϕ.

We now construct the equations of motion. This is more subtle than simply substituting in the derivatives, so we step through the process carefully. Begin by noting that the equation for $\bar{\Gamma}$, which contains no derivatives, is unchanged by the coordinate transformation. The evolution equations for $\tilde{R}$ and $\tilde{m}$ are straightforward to compute by substituting in expressions for the invariant derivatives.

$$\partial_{\bar{u}}\tilde{R} = e^{\psi-\xi}\left(\tilde{U} - e^{-\phi}\tilde{R}\right) \tag{161}$$

eq:partialuR

$$\partial_{\bar{u}}\tilde{m} = 3e^{\psi-\xi}\left((1+w)e^{-\phi}\tilde{m} - \frac{\tilde{U}}{\tilde{R}}(\tilde{P}+\tilde{m})\right) \tag{162}$$

Here, we've defined the dimensionless coordinate $\bar{u} = u/R_H$, which absorbs all factors of R_H in the equations of motion.

Noting that

$$\Gamma = D_r R = e^{-\lambda/2}\frac{\partial R}{\partial A}\bigg|_u - D_t R \tag{163}$$

and further that $U = D_t R$, we obtain

$$e^{\lambda/2} = \frac{\partial_A R\big|_u}{\Gamma + U}. \tag{164}$$

Substituting in our cosmological variables, this becomes

$$e^{\lambda/2} = e^{\xi}\frac{\alpha\tilde{R}\xi' + \tilde{R}'}{\bar{\Gamma}+\tilde{U}} \tag{165}$$

eq:lambdahm

where we let $X' = \partial_{\bar{A}}X\big|_u$. The RHS is comprised of known quantities, so this allows us to compute $e^{\lambda/2}$.

Next, we look at understanding the behavior of ξ. From Eq. (137), at constant A we have

$$\frac{\partial t}{\partial u}\bigg|_A = e^{\psi-\phi}. \tag{166}$$

Substituting in $t = \alpha R_H e^{\xi}$ and $u = R_H\bar{u}$, this becomes

$$\partial_{\bar{u}}\xi = \frac{1}{\alpha}e^{\psi-\phi-\xi}. \tag{167}$$

This is the evolution equation for ξ. If we instead look at constant u, we obtain

$$\frac{\partial t}{\partial A}\bigg|_u = e^{\lambda/2-\phi}. \tag{168}$$

Again substituting in for t and also for $A = R_H\bar{A}$, we obtain

$$e^{\phi} = \frac{e^{\lambda/2-\xi}}{\alpha\xi'}. \tag{169}$$

eq:ephiHM

The RHS is again completely known, so this allows us to compute e^{ϕ}, which appears in all of the evolution equations.

We now tackle $\tilde{\rho}$. Here, it is most instructive to proceed from $D_k m$, as in Eq. (153).

$$e^{-\lambda/2}\partial_A m\big|_u = 4\pi R^2(\rho\Gamma - PU) \tag{170}$$

Substituting in for the tilded variables, this becomes

$$e^{-\lambda/2}\partial_{\bar{A}}\left(e^{(3\alpha-2)\xi}\tilde{R}^3\tilde{m}\right) = 3e^{3(\alpha-1)\xi}\tilde{R}^2\tilde{\rho}(\bar{\Gamma} - w\tilde{U}). \tag{171}$$

Solving for $\tilde{\rho}$, we obtain

$$\tilde{\rho} = \frac{e^{3(1-\alpha)\xi}e^{-\lambda/2}}{3\tilde{R}^2(\bar{\Gamma}-w\tilde{U})}\partial_{\bar{A}}\left(e^{(3\alpha-2)\xi}\tilde{R}^3\tilde{m}\right). \tag{172}$$

eq:hmrhoeq

While the chain rule can be used on the RHS, we leave it written in this manner to aid with the numerical computation of derivatives.

By working in Misner-Sharp coordinates, we can compute

$$D_r\tilde{R} = \frac{1}{aR_H}e^{-\lambda/2}\partial_a R\big|_t = \frac{\Gamma}{aR_H} = \frac{e^{-\xi}\bar{\Gamma}}{R_H} \tag{173}$$

eq:cleverDrR

which by the invariance of D_r, must be the same in the new coordinate system. This is particularly useful when computing the evolution equation for $\tilde{U}$.

Finally, we come to the evolution equation for $\tilde{U}$. Transforming the derivatives and substituting Eq. (173) for $D_R\tilde{R}$ yields

$$e^{-\psi}\partial_{\bar{u}}\tilde{U} = e^{-\xi}\left(\frac{1-\alpha}{\alpha}e^{-\phi}\tilde{U} - \frac{\tilde{R}}{2}\left(\tilde{m}+3\tilde{P}\right)\right) - \frac{\bar{\Gamma}w}{\tilde{\rho}(1+w)}(e^{-\lambda/2}\tilde{\rho}' - e^{-\psi}\partial_{\bar{u}}\tilde{\rho}). \quad (174)$$

This needs an evolution equation for $\tilde{\rho}$. To obtain this, start by writing Eq. (48) in terms of invariant derivatives.

$$\alpha R_H e^{\phi+\xi} D_t\tilde{\rho} = 2\tilde{\rho}\left[1 - \frac{1}{3}e^{\phi}\left(\frac{2\tilde{U}}{\tilde{R}} + \frac{D_r\tilde{U}}{D_r\tilde{R}}\right)\right]. \quad (175)$$

Substituting for the invariant derivatives, we obtain

$$e^{-\psi}\partial_{\bar{u}}\tilde{\rho} = \frac{2}{\alpha}e^{-\xi}\tilde{\rho}\left(e^{-\phi} - \frac{2\tilde{U}}{3\tilde{R}}\right) - \frac{\tilde{\rho}(1+w)}{\bar{\Gamma}}(e^{-\lambda/2}\tilde{U}' - e^{-\psi}\partial_{\bar{u}}\tilde{U}). \quad (176)$$

Substituting this back into Eq. (174) leads to

$$e^{-\psi}\partial_{\bar{u}}\tilde{U} = e^{-\xi}\left(\frac{1-\alpha}{\alpha}e^{-\phi}\tilde{U} - \frac{\tilde{R}}{2}\left(\tilde{m}+3\tilde{P}\right)\right) + 3w\bar{\Gamma}e^{-\xi}\left[e^{-\phi} - \frac{2\tilde{U}}{3\tilde{R}} - \frac{\alpha}{2}e^{\xi-\lambda/2}\frac{\tilde{\rho}'}{\tilde{\rho}}\right] - w(e^{-\lambda/2}\tilde{U}' - e^{-\psi}\partial_{\bar{u}}\tilde{U}). \quad (177)$$

Finally, this can be solved for $\partial_{\bar{u}}\tilde{U}$.

$$\partial_{\bar{u}}\tilde{U} = \frac{e^{\psi-\xi}}{1-w}\left[\frac{1-\alpha}{\alpha}e^{-\phi}\tilde{U} - \frac{\tilde{R}}{2}\left(\tilde{m}+3\tilde{P}\right) - we^{\xi-\lambda/2}\tilde{U}' + 3w\bar{\Gamma}\left(e^{-\phi} - \frac{2\tilde{U}}{3\tilde{R}} - \frac{\alpha}{2}e^{\xi-\lambda/2}\frac{\tilde{\rho}'}{\tilde{\rho}}\right)\right]. \quad (178)$$

To summarize, at each time step, a number of auxiliary variables must first be computed, and ψ must be integrated.

$$\bar{\Gamma}^2 = e^{2(1-\alpha)\xi} + \tilde{U}^2 - \tilde{R}^2\tilde{m} \quad (179a)$$

$$e^{\lambda/2} = e^{\xi}\frac{\alpha\tilde{R}\xi' + \tilde{R}'}{\bar{\Gamma}+\tilde{U}} \quad (179b)$$

$$e^{\phi} = \frac{e^{\lambda/2-\xi}}{\alpha\xi'} \quad (179c)$$

$$\tilde{\rho} = \frac{e^{3(1-\alpha)\xi}e^{-\lambda/2}}{3\tilde{R}^2(\bar{\Gamma}-w\tilde{U})}\partial_{\bar{A}}\left(e^{(3\alpha-2)\xi}\tilde{R}^3\tilde{m}\right) \quad (179d)$$

$$\partial_{\bar{A}}\ln\left(e^{-\psi}(\bar{\Gamma}+\tilde{U})\right) = \xi'\left(1-\alpha-\frac{e^{\phi}\tilde{R}\tilde{\rho}}{\bar{\Gamma}+\tilde{U}}\right) \quad (179e)$$

Once all auxiliary variables are in place, the evolution equations may then be computed.

$$\partial_{\bar{u}}\xi = \frac{1}{\alpha}e^{\psi-\phi-\xi} \quad (180a)$$

$$\partial_{\bar{u}}\tilde{R} = e^{\psi-\xi}\left(\tilde{U} - \tilde{R}e^{-\phi}\right) \quad (180b)$$

$$\partial_{\bar{u}}\tilde{m} = 3e^{\psi-\xi}\left((1+w)e^{-\phi}\tilde{m} - \frac{\tilde{U}}{\tilde{R}}(\tilde{P}+\tilde{m})\right) \quad (180c)$$

$$\partial_{\bar{u}}\tilde{U} = \frac{e^{\psi-\xi}}{1-w}\left[\frac{1-\alpha}{\alpha}e^{-\phi}\tilde{U} - \frac{\tilde{R}}{2}\left(\tilde{m}+3\tilde{P}\right) - we^{\xi-\lambda/2}\tilde{U}' + 3w\bar{\Gamma}\left(e^{-\phi} - \frac{2\tilde{U}}{3\tilde{R}} - \frac{\alpha}{2}e^{\xi-\lambda/2}\frac{\tilde{\rho}'}{\tilde{\rho}}\right)\right]. \quad (180d)$$

Note that when the lapse $e^{\psi} \to 0$ near horizon formation, all quantities are frozen.

There are two denominators to be wary of here. The first, $\bar{\Gamma}+\tilde{U} \propto U+\Gamma$ is of no concern, as $\Gamma+U$ is always positive in this coordinate system. The second, $\bar{\Gamma}-w\tilde{U}$, is of more concern. As can be seen from Eq. (153), this combination arises from

$$D_k m = 4\pi\rho R^2(\Gamma - wU) \propto \rho(\bar{\Gamma} - w\tilde{U}). \quad (181)$$

where it is not guaranteed that $\Gamma - wU$ is positive. At sufficiently large radii, the derivative of m along the outgoing null ray can become negative. However, as ρ is always positive, $D_k m$ and $\Gamma - wU$ must vanish at the same point.

For the background FRW evolution, this crossover occurs at $R = 1/(wH)$. If we start a null ray at $R = 0$ at $\xi = 0$, its position in comoving coordinates is given by

$$\bar{A}(\xi) = \frac{\alpha}{1-\alpha}[e^{(1-\alpha)\xi} - 1]\,. \quad (182)$$

When the null ray hits the boundary $\bar{A}_*$ at ξ_*, we have

$$\frac{1-\alpha}{\alpha}\bar{A}_* + 1 = e^{(1-\alpha)\xi_*}\,. \quad (183)$$

The crossover radius for the FRW background at time ξ_* is

$$\bar{A}_c = \frac{1}{w}e^{(1-\alpha)\xi_*} = \frac{1}{w}\left[1 + \frac{1-\alpha}{\alpha}\bar{A}_*\right]\,. \quad (184)$$

For $w = 1/3$ ($\alpha = 1/2$), this yields $\bar{A}_c = 1 + 3\bar{A}_*$, and the crossover point should be well outside of the domain. So long as the evolution begins with linear initial data, this result should continue to be roughly correct.

In the Misner-Sharp formalism, we had the boundary condition $\partial_{\bar{A}}\tilde{X} = 0$ at the origin for $\tilde{m}$ and $\tilde{\rho}$. This translates to the coordinate invariant condition $D_r\tilde{X} = 0$ at the origin. In the Hernandez-Misner formalism, this condition yields

$$\partial_{\bar{u}}\tilde{X} = e^{\psi-\lambda/2}\partial_{\bar{A}}\tilde{X} \quad (185)$$

at the origin. The boundary conditions that $\tilde{R} = \tilde{U} = 0$ at the origin remain unchanged, although one should note that these are no longer odd functions, as extending through to negative radius continues to extend backwards in time!

The Hernandez-Misner formalism was originally formulated to describe a collapsing object surrounded by vacuum in an asymptotically flat spacetime. The time coordinate was taken to be the clock time of a static asymptotic observer at spacelike infinity. As we do not have an asymptotically flat spacetime, such an observer doesn't exist. Instead, we place an observer at the boundary of the computational domain. It is convenient to choose u to track the cosmological time of this observer. By the differential relation (137) with $dA = 0$, we have

$$\left.\frac{\partial u}{\partial t}\right|_A = e^{\phi-\psi} = 1\,, \tag{186}$$

and so we demand that $\phi = \psi$ on the outer boundary. This is best done by using the value of ϕ computed from Eq. (179c).

Constructing outer boundary conditions is more complicated. As the null slicing guarantees that there are two ingoing characteristics at the outer boundary, our previous results from the linear analysis are unable to provide an appropriate wave boundary condition. The most stable outer boundary condition we found was to impose the Dirichlet boundary condition $\tilde{\rho} = \text{const}$, where the constant was determined by the initial conditions on the slice. While this tended to inject some energy into the system, there is no effect on the black hole mass so long as the outer boundary is causally disconnected from the collapsing region.

C. Initial Data

One issue with the Hernandez-Misner approach is that initial data is typically not provided along a null slice. As such, it is typical to use the Misner-Sharp formalism to evolve a set of initial conditions, recording initial data along a null geodesic as the evolution progresses.

During the Misner-Sharp evolution, in addition to evolving the physical variables, compute the trajectory of a null ray starting at the origin, described by

$$\partial_\xi \bar{A} = \alpha e^{\phi} \frac{\bar{\Gamma}}{\partial_{\bar{A}} \tilde{R}} \tag{187}$$

in our variables. The initial condition is that the geodesic begins at the origin, $\bar{A}(\xi = 0) = 0$. After each time step, record the $\bar{A}$ position of the null geodesic, the values for $\tilde{m}$, $\tilde{U}$ and $\tilde{R}$, as well as the time ξ.

If no black hole forms, then the Hernandez-Misner formalism is not required. If a black hole does form, then the domain can be truncated, excising the black hole, and evolution continued until the null ray reaches the outer boundary of the computational domain. As no inner boundary condition can be known for the truncated domain, we suggest repeatedly truncating the domain to remove unphysical artifacts. From experimentation, we found that setting a Dirichlet boundary condition of constant $\tilde{\rho}$ at the inner boundary worked well to stabilize the boundary. Note that what occurs at the inner boundary cannot causally affect the evolution at the location of the null geodesic, as the speed of sound in the fluid is less than the speed of the light. Once the null ray reaches the outer boundary, the data along this ray can be used as the initial conditions for the Hernandez-Misner formalism. The initial value of $\bar{u}$ can be set using $\bar{u} = \alpha e^{\xi(\bar{A}_{\max})}$.

FIXME: I've implemented the new definition of $\tilde{U}$ up to this point. This section has not been edited at all, going forwards.

D. Mass Extraction

The black hole formation condition in the Hernandez-Misner formalism is the same as in the Misner-Sharp formalism (Eq. (52)):

$$\frac{2m}{R} \equiv \tilde{R}^2 \tilde{m} e^{2(\alpha-1)\xi} \geq 1 \quad \text{and} \quad \tilde{U} < 0\,. \tag{188}$$

Of course, this condition is never met: when it comes close, the evolution is suppressed by the vanishing of the lapse. We thus need a method by which to extract the black hole mass. The method we describe here is based on that suggested by Baumgarte *et al.* [36], and demonstrated on an evolution that started with a Gaussian initial profile (see Section VII for full details).

In Fig. 2, we plot the quantity $2m/R$ as a function of areal radius. We see that as the black hole gets closer to forming, the curve approaches but never reaches the formation condition. In our simulations, we found that $2m/R$ typically grew to larger than 0.995 before we terminated the evolution.

Figure 3 shows a plot of the lapse as a function of areal radius. We see that as the black hole forms, the lapse essentially vanishes at a reasonably well-defined radius. The inset shows that the lapse approaches zero exponentially quickly.

In order to extract the black hole mass, we first find the radius at which the lapse starts to vanish. Programmatically, we chose to wait until the lapse at the origin satisfied $e^{\psi} \leq 10^{-10}$ (alternatively, waiting for $2m/R > 0.995$ at some position is also reasonable). When this occurs, we find the areal radius R_0 at which the lapse $e^{\psi} = 10^{-6}$. As the lapse is basically falling vertically at this point, it doesn't particularly matter if you choose 10^{-4}, 10^{-6} or 10^{-8} for the purpose of computing R_0.

In Fig. 4, we plot the function $m(R)$ as a function of R. Note the sharp elbow that occurs near $R = R_0$. After

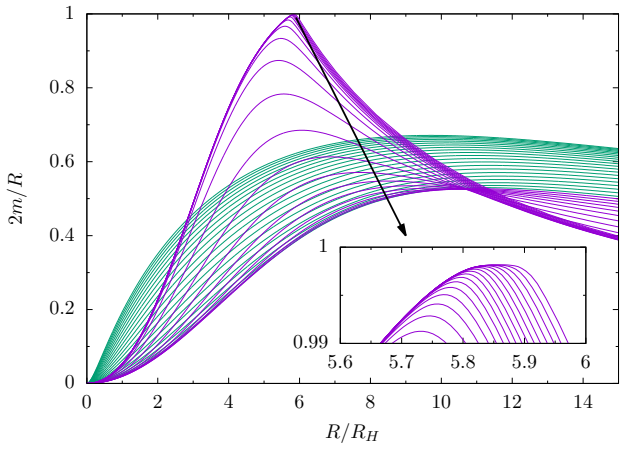

Figure 2. $2m/R$ as a function of areal radius. The black hole formation condition is $2m/R \geq 1$. In the inset, we plot the behavior near the formation condition. The lines in teal are earlier lines, and the lines in purple are taken at later times. We see that the formation condition is almost met at late times. The colors are used simply to help show the evolution.

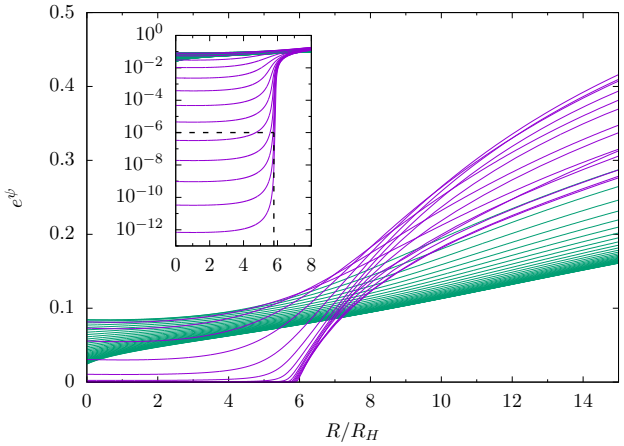

Figure 3. The lapse e^{ψ} as a function of areal radius. As with the previous figure, lines in teal are early, while lines in purple are later. The inset contains the same plot, but on a log scale. We see that as the black hole forms, the lapse plummets, essentially freezing evolution. A horizontal dashed black line is drawn at the 10^{-6} level, and the corresponding radius R_0 for mass extraction is read off from the vertical dashed black line.

this elbow, m is essentially constant in radius, indicating that the black hole has consumed all of the nearby matter. We can read off the mass of the black hole from any point past the elbow (as everything near the elbow will fall in). We suggest using[10] $R = 1.1\, R_0$.

[10] Note that once R_0 has been found, one can estimate the black hole mass as $M = R_0/2$. However, doing so will neglect any fluid floating just outside the event horizon, which should be included in the mass estimate.

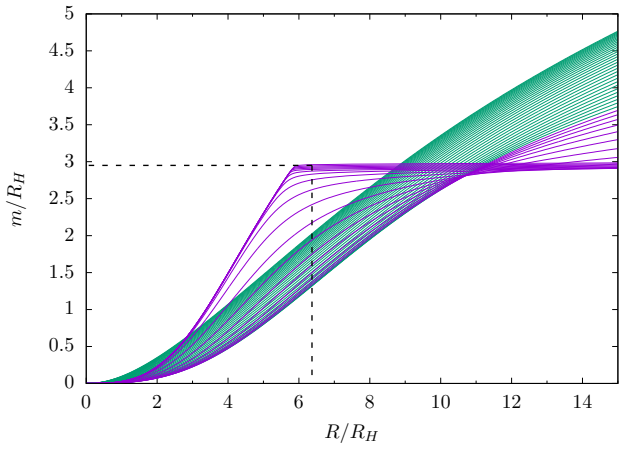

Figure 4. Mass enclosed in areal radius R as a function of R. As with the previous plots, earlier timesteps are in teal, while later timesteps are in purple. We see that when the black hole forms, it consumes all the nearby matter, and m becomes constant in radius. If you extract the black hole mass at $R = 6R_H$ or $R = 10R_H$, you will find essentially the same mass. Off the right of the plot, m starts increasing again. A vertical dashed black line is drawn at $1.1R_0$ (with R_0 extracted from the previous figure), and the mass contained in the black hole is read off from the corresponding horizontal dashed black line.

Once the black hole has formed, it very slowly accretes mass, as evidenced by the slowly rising horizontal line of the black hole mass in Fig. 4. As this process is somewhat slow, it can be ignored for the purposes of estimating the final black hole mass. So long as one is consistent in the mass extraction procedure, the amount of accretion after initial formation should just be a small systematic error. There is no "final" resulting mass, as black holes will continuously accrete from the surrounding cosmology.

In terms of our variables, the resulting mass is written as

$$m = \frac{1}{2} e^{(3\alpha-2)\xi} \tilde{R}^3 \tilde{m} R_H \,. \tag{189}$$

Once the extraction radius is known, it needs to be translated into a value for $\tilde{R}$ and then $\bar{A}$, so that ξ and $\tilde{m}$ can be found.

Note that the mass is written in terms of the initial horizon radius. In order to compare this to more useful mass scales, we consider the mass within the horizon in an FRW universe.

$$m_{horizon}(\xi) = \frac{1}{2} e^{\xi} R_H \tag{190}$$

It is typical to compare the mass of the black hole with the mass contained in the horizon at the time ξ_0 when

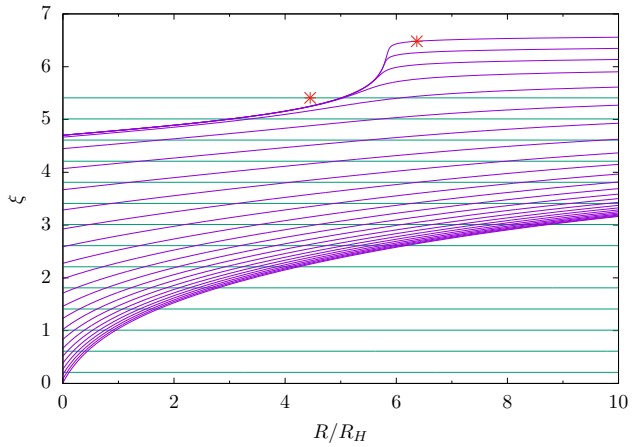

Figure 5. Constant time slices in Misner-Sharp (teal) coordinates and constant u slices in Hernandez-Misner (purple) coordinates, plotted against areal radius. The Misner-Sharp simulation was run until the simulation could not proceed any further due to singularity formation at the origin. A red mark is placed at the outermost trapped surface on the final time slice, from which the mass of the black hole can be estimated. A second red mark is placed on the position at which the black hole mass was extracted from the Hernandez-Misner formalism. Note that the position of the event horizon can be inferred from the purple slices.

the perturbation enters the horizon. This time will need to be extracted from the Misner-Sharp evolution. Taking this ratio then eliminates R_H.

For the example presented here, we find $R_0 = 5.79R_H$. This radius corresponds to a mass of $2.89R_H$, while $1.1R_0$ corresponds to a mass of $2.95R_H$. From looking at the Misner-Sharp data, we found that the perturbation entered the horizon at $\xi = 2.47$. The ratio of the black hole mass to the mass enclosed in the horizon at the time of horizon crossing is then

$$\frac{m_{black\ hole}}{m_{horizon\ crossing}} = 0.50. \tag{191}$$

If you do not wish to go to the effort of getting the Hernandez-Misner formalism to run, you can always simply estimate the mass of the black hole from the Misner-Sharp formalism: just leave the evolution to run until it dies from an inability to evolve further (due to the formation of a singularity). Then, find the outermost trapped surface, and read off the mass from there.

This method will always underestimate the black hole mass, as a fair amount of matter will fall through the horizon soon after its formation. For the example we have provided here, the mass we extracted from the Misner-Sharp evolution before the simulation died was $m = 2.25R_H$, substantially less than the mass from the Hernandez-Misner formalism. We expect that the deficit is strongly dependent upon the initial density profile.

In Fig. 5, we plot constant time slices in Misner-Sharp coordinates and constant u slices in Hernandez-Misner coordinates. The spacetime events from where the Misner-Sharp and Hernandez-Misner mass estimates are extracted are also indicated. The figure also demonstrates that the Hernandez-Misner coordinates do an impressive job of hugging the event horizon, and that the Misner-Sharp coordinates can be used to probe a little bit inside the horizon.

E. FRW Evolution

For code debugging purposes, it is useful to know analytic forms for all the variables in the case of pure FRW evolution. In particular, $\tilde{m} = \tilde{\rho} = e^{\phi} = 1$ and $\tilde{R} = \tilde{U} = \bar{A}$. It is straightforward to check that this is preserved under the evolution equations (180). Furthermore, $\Gamma = 1$, $e^{\lambda/2} = a = e^{\alpha\xi}$ and $\bar{\Gamma} = e^{(1-\alpha)\xi}$. All that remains to be computed is $\xi(\bar{A}, \bar{u})$ and $e^{\psi(\bar{A},\bar{u})}$.

We begin with ξ. From Eq. (179c), we find

$$\partial_{\bar{A}} e^{(1-\alpha)\xi} = \frac{1-\alpha}{\alpha}. \tag{192}$$

Our coordinate system is constructed in such a way that on the outer boundary, $t(\bar{A}_{\max}, \bar{u}) = \bar{u}$, and so

$$e^{\xi(\bar{A}_{\max},\bar{u})} = \frac{\bar{u}}{\alpha}. \tag{193}$$ eq:initial

Therefore,

$$e^{(1-\alpha)\xi} = \frac{1-\alpha}{\alpha}(\bar{A} - \bar{A}_{\max}) + \left(\frac{\bar{u}}{\alpha}\right)^{1-\alpha}. \tag{194}$$ eq:xifrw

Looking towards ψ, from Eq. (151), we obtain

$$\partial_{\bar{A}}\psi = e^{(\alpha-1)\xi} \tag{195}$$

after some substitutions. We can use Eq. (194) to integrate this, yielding

$$e^{\psi} = \left(1 + \frac{1-\alpha}{\alpha}\frac{\bar{A} - \bar{A}_{\max}}{\left(\frac{\bar{u}}{\alpha}\right)^{1-\alpha}}\right)^{\alpha/(1-\alpha)} \tag{196}$$

where we fix the constant of integration by demanding that $e^{\psi} = e^{\phi} = 1$ at $\bar{A}_{\max}$.

In the Misner-Sharp formalism, doubling the size of the domain (i.e., doubling $\bar{A}_{\max}$) while maintaining the same resolution roughly doubles the computational time. In the Hernandez-Misner formalism, this is no longer the case. Starting with Eq. (194), let $\xi_0 = \xi(0, \bar{u})$ be the time at the origin, and invert to obtain $\bar{u}(\xi_0)$. For illustration purposes, we use $\alpha = 1/2$ and $w = 1/3$.

$$\bar{u}(\xi_0) = \frac{1}{2}\left(e^{\xi_0/2} + \bar{A}_{\max}\right)^2 \tag{197}$$

If we consider the change in $\bar{u}$ between ξ_0 and $\xi_0 + \epsilon$, we find

$$\bar{u}(\xi_0 + \epsilon) - \bar{u}(\xi_0) = \frac{1}{2} e^{\xi_0/2} (\bar{A}_{\max} + e^{\xi_0/2}) \epsilon + O(\epsilon^2). \tag{198}$$

For early times, this will be roughly proportional to $\bar{A}_{\max}$, and so increasing the radius of the outer boundary also increases the amount of effort that needs to be expended in taking a time step in ξ_0. Further note that all of this extra effort only goes into evolving the region between the old and the new $\bar{A}_{\max}$, which is typically not the region of interest!

This problem is magnified when a black hole is forming, as the lapse near the origin becomes increasingly small, and large steps in $\bar{u}$ are required to achieve very small steps in ξ_0 near the origin. Hence, taking a large domain is much more computationally expensive in the Hernandez-Misner formalism. When transitioning to the Hernandez-Misner formalism, we suggest choosing an outer boundary at a reasonable location, possibly at a radius less than the outer boundary for the Misner-Sharp evolution.

VI. CODING ISSUES

In this section, we detail various issues pertaining to coding the formalism presented here.

A. Grids and Derivatives

As shocks can form in this formalism, a finite difference method is needed for spatial derivatives rather than spectral methods. For the Misner-Sharp formalism, we found it useful to not have a gridpoint at the origin (having a grid at $h/2$, $3h/2$, etc), and instead used the even/odd nature of the variables to compute derivatives and enforce the boundary conditions. In the Hernandez-Misner formalism, placing a gridpoint at the origin makes enforcing the boundary conditions simpler.

In both the Misner-Sharp and Hernandez-Misner formalisms, the spatial coordinate $\bar{A}$ never explicitly appears, and all derivatives with respect to $\bar{A}$ appear as ratios of derivatives. This is a reflection of the reparametrization invariance of the formalisms. Due to this, we found it convenient to eliminate $\bar{A}$ altogether, simply using it as a gridpoint index. All spatial derivatives are then effectively derivatives with respect to $\tilde{R}$.

Due to the use of comoving coordinates, the gridpoints continually change their radius. During black hole formation, there is typically a large amount of grid distortion, which can lead to large errors in derivatives. While some authors have addressed this through adaptive mesh refinement, a much simpler way is to simply insert some extra gridpoints when derivatives become inaccurate (so-called "regridding").

In the Misner-Sharp formalism, one must be careful about the implementation of the derivative $\tilde{\rho}'$ to ensure that the differentiation operator maintains a negative definite spectrum. The most accurate derivative operator we found was

$$\tilde{\rho}' = \frac{4}{3} \frac{\partial}{\partial(\tilde{R}^4)} (\tilde{R}^4 \partial_{\tilde{R}} \tilde{m}) \tag{199}$$

written as a centered difference of a forward/backward derivative (2nd order in accuracy on a uniform grid). Care must also be taken in the Hernandez-Misner formalism, where a similar approach is recommended for computing derivatives of $\tilde{\rho}$ in the form of Eq. (172).

For time stepping, we had success using the method of lines with a DOPRI 5-4 Runge-Kutta algorithm. Using our laptops, the Misner-Sharp formalism could typically determine if a black hole formed or not in a few seconds, while the Hernandez-Misner formalism could take a few minutes to extract the black hole mass.

For the domain size, we saw above that having $\bar{A}_{max}$ be too large would lead to a very slow evolution for Hernandez-Misner. On the other hand, having $\bar{A}_{max}$ be too small may lead to the outer boundary being in causal contact with the collapsing region, in which case the pinned boundary condition can lead to erroneous results. While the optimal size of $\bar{A}_{max}$ depends on the width of the initial perturbation, we found that a reasonable rule of thumb was to let $\bar{A}_{max}$ be ~ 10 times larger than the initial perturbation.

B. Timestep Limits

The Courant-Friedrichs-Lewy (CFL) condition [58] provides a limit to the size of a timestep that can be taken in a numerical evolution. Here, we provide the limit in both the Misner-Sharp and Hernandez-Misner formalisms [36].

The system we are evolving has two characteristics that propagate inwards and outwards with speed of sound $c_s = dA/dt = \sqrt{w} e^{\phi - \lambda/2}$ in Misner-Sharp coordinates, or

$$\frac{d\bar{A}}{d\xi} = \alpha \sqrt{w} e^{\phi + \xi - \lambda/2} = \frac{\alpha \sqrt{w} e^{\phi} \bar{\Gamma}}{\tilde{R}'} \tag{200}$$

in our cosmological coordinates. The CFL condition thus requires

$$\frac{\alpha \sqrt{w} e^{\phi} \bar{\Gamma}}{\tilde{R}'} < \frac{\Delta \bar{A}}{\Delta \xi} \tag{201}$$

where $\Delta \bar{A}$ is the grid spacing and $\Delta \xi$ is the amount of time being stepped forwards. This reduces to the condition

$$\Delta \xi < \frac{\tilde{R}' \Delta \bar{A}}{\alpha \sqrt{w} e^{\phi} \bar{\Gamma}} = \frac{\Delta \tilde{R}}{\alpha \sqrt{w} e^{\phi} \bar{\Gamma}}. \tag{202}$$

Note that $\bar{\Gamma} \sim e^{2(1-\alpha)\xi}$ in the linear regime, and hence the CFL condition requires the timestep to shrink as time increases.

In the Hernandez-Misner formalism, we can use the discrete form of Eq. (137) to obtain[11]

$$e^{\phi}\Delta t = e^{\psi}\Delta u + e^{\lambda/2}\Delta A\,. \tag{203}$$

Writing $\Delta t = \alpha\Delta\xi/H$ and using $\Delta\xi$ from above, we obtain

$$\Delta\bar{u} < \left(\frac{1}{\sqrt{w}} - 1\right) e^{\lambda/2-\psi}\Delta\bar{A}\,. \tag{204}$$

Using Eq. (165) to transform to differences in $\tilde{R}$, this becomes

$$\Delta\bar{u} < \left(\frac{1}{\sqrt{w}} - 1\right) e^{\xi-\psi}\frac{\alpha\tilde{R}\partial_{\bar{R}}\xi + 1}{\bar{\Gamma} + \tilde{U}}\Delta\tilde{R}\,. \tag{205}$$

The CFL condition is a necessary but insufficient condition on stability. Further conditions on timestepping in the Misner-Sharp and Hernandez-Misner formalisms have been used in the literature [22, 36], including limiting density changes to $\Delta\rho/\rho < 0.02$, radius changes to $\Delta R/R < 0.005$, and changes in the quantity $1-2m(R)/R$ to less than 0.1. Sometimes, these conditions can be much more stringent than the CFL condition. We found that it was typically sufficient to just impose the CFL condition and otherwise let the adaptive time stepper from the Runge-Kutta library determine when particularly small time steps were necessary.

C. Artificial Viscosity

FIXME: Need to address this section!

In our equations of motion, we included artificial viscosity from the very beginning, although we never gave it a form. We finally come to address this issue.

Artificial viscosity is an additional pressure that is added into the system in order to mitigate the formation of shocks. The original implementations of the Misner-Sharp and Hernandez-Misner formalism included artificial viscosity in their equations of motion, and subsequent investigations of supernovae collapse also utilized it. Papers in the literature using these formalisms for primordial collapse have sometimes implemented it, but documentation has been somewhat scarce.

Shocks occur when a discontinuity forms in a curve, which leads to wildly inaccurate spatial derivatives. The idea of artificial viscosity is to add extra pressure when a shock looks likely to form in order to smooth out the discontinuity. However, we note that both the Misner-Sharp and particularly the Hernandez-Misner formalisms are capable of producing very steep derivatives that are nonetheless continuous, and simply require additional gridpoints to resolve; artificial viscosity does nothing to help in this situation.

We found that outgoing shocks tended to form in the Misner-Sharp formalism when an overdensity failed to collapse into a black hole, and artificial viscosity was useful for smoothing these over. We also observed ingoing shocks arising from somewhat unrealistic initial data. We recommend implementing artificial viscosity in the Misner-Sharp formalism, where it is effective at mitigating shock formation.

For the Hernandez-Misner formalism, shocks are much less likely to form, as outgoing shocks typically preclude the formation of a black hole. Furthermore, the vanishing lapse tends to ensure that everything freezes around the region of interest when a black hole forms. Finally, the inclusion of artificial viscosity significantly complicates the equations of motion. We recommend ignoring artificial viscosity in this formalism, noting that a few other authors have done likewise [44, 49]. We direct the interested reader to Baumgarte *et al.* [36] if implementation details are desired.

We now describe our implementation of artificial viscosity for the Misner-Sharp formalism. The origin of the form of dissipation that we describe goes back to Neumann and Richtmyer [52], which has been used in many evolutions of this kind [22, 36, 45, 59–61]. The basic idea is to identify where sharp discontinuities may occur, and artificially increase the pressure there in order to smear out the discontinuity over a few gridpoints.

We investigated two triggers for identifying when to turn on artificial viscosity. The first condition, used by May and White [60], is to trigger on $\partial_t\rho > 0$. The second condition, used by Baumgarte *et al.* [36] (BST), instead triggers on $\partial_A U < 0$. Both of these triggers seem reasonable: in the first instance, if the density is increasing, then something is collapsing. In the second instance, the idea is to identify shocks (moving in either direction) as requiring a negative velocity gradient.

The suggested form of the viscosity term is

$$P_{vis} = \begin{cases} \kappa\rho(\Delta A\partial_A U)^2 & \text{when triggered} \\ 0 & \text{otherwise} \end{cases} \tag{206}$$

where κ is a dimensionless constant that controls the strength of the viscosity, ΔA is the grid spacing, and we take derivatives at constant t.

In our description, we can construct $\tilde{Q}$ as

$$\tilde{Q} = \kappa(\Delta\bar{A})^2 e^{2(\alpha-1)\xi}\left[\partial_{\bar{A}}\left(\tilde{R}\tilde{U}\right)\right]^2\,. \tag{207}$$

The two triggering conditions become

$$\tilde{R}'\tilde{U} < -\frac{\tilde{R}\tilde{U}'}{3} \quad \text{(May and White)} \tag{208a}$$

$$\tilde{R}'\tilde{U} < -\tilde{R}\tilde{U}' \quad \text{(BST)} \tag{208b}$$

[11] Note that this is the outgoing characteristic. The incoming characteristic uses $-\Delta A$ instead, but provides a less stringent bound.

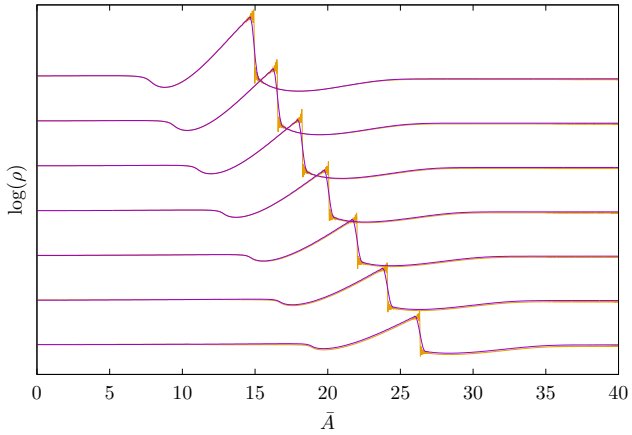

Figure 6. Density profiles from two Misner-Sharp evolutions from the same initial data. These evolutions did not form a black hole, but sent out a spherical wave of matter, which will tend to form a shock. In the purple evolution, artificial viscosity was turned on with $\kappa = 2$, while in the yellow evolution, artificial viscosity was turned off. The manner in which artificial viscosity has smoothed the shock is evident. FIXME: Change to $\tilde{R}$

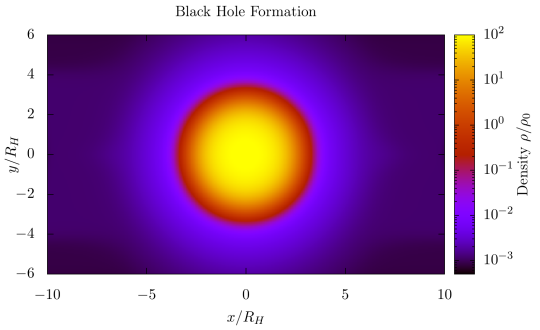

Figure 7. Still frame taken from an animation describing the formation of a black hole in spherical symmetry. FIXME: Remove

where we use Eq. (20) for the first condition, and note that $\tilde{R}' > 0$ by Eq. (103). Despite rather different origins, these conditions are very similar. Indeed, the two conditions are equivalent to taking the divergence of U in spherical polar coordinates ($\partial_{\bar{A}}(R^2 U) < 0$) or in a linear sense ($\partial_{\bar{A}} U < 0$). When the velocities are converging instead of diverging, the viscosity triggers.

We found that the BST trigger tended to work better than the May and White trigger. As a curious side effect, we observed that the smoothing provided by the artificial viscosity increased the performance of our outer boundary condition. The effects of artificial viscosity are evident in Fig. 6, where we show data from evolutions with the same initial data, but with $\kappa = 2$ and $\kappa = 0$. In general, we found that $\kappa \simeq 2$ is a reasonable value of the coefficient.

FIXME: This will need to change based on the $\tilde{R}$ spacing, given that we've recommended eliminating $\bar{A}$ altogether.

When artificial viscosity is activated, the lapse e^{ϕ} cannot by computed from a simple power of ρ, and instead must be integrated. To avoid integration error, we recommend implementing it as follows. Let

$$\phi' = -\frac{P'}{\rho + P} = -\frac{w\rho'}{(1+w)\rho} + \left(\frac{w\rho'}{(1+w)\rho} - \frac{P'}{\rho + P} \right). \tag{209}$$

The first term can be integrated analytically, and the second term can be integrated numerically:

$$\phi = -\frac{w}{1+w} \ln(\rho) - \int_{\bar{A}}^{\bar{A}_{\max}} \left[\frac{w\rho'}{(1+w)\rho} - \frac{P'}{\rho + P} \right] d\bar{A}\,. \tag{210}$$

The integrand only has nonzero support when $Q \neq 0$. We then have

$$e^{\phi} = \rho^{-w/(1+w)} \exp\left[\int_{\bar{A}}^{\bar{A}_{\max}} \left(\frac{w\rho'}{(1+w)\rho} - \frac{P'}{\rho + P} \right) d\bar{A} \right]. \tag{211}$$

VII. IMPLEMENTATION EXAMPLES

In this section, we discuss animations from simulations of the formalism that we have described in this paper[12]. We have included still frames from the animations in this paper, but we believe that the animations provide a much better picture of the evolution than these frames can describe. For the benefit of those only interested in understanding the animations, we include a brief summary of the formalisms.

A. Density Animations

We start our animations with a 2D density map that evolves in time to form a black hole ("Black Hole Formation"). This animation requires no understanding of our formalism to interpret, and gives a good idea of how a black hole can form in the early universe. The expansion of the universe and the corresponding dilution of energy is evident as the map evolves, before the density collapses to form a black hole. The animation runs through twice; the first cycle shows the density using a linear scale, while the second cycle uses a logarithmic scale. A still frame from the end of the logarithmic version is shown in Fig. 7.

[12] These animations may be found in the supplemental materials associated with this paper on the arXiv, and also in a playlist on youtube at `http://www.youtube.com/playlist?list=PLqRPTTDr7yKTD9HExr7Fgk_RVrg5RwTau`.

B. Misner-Sharp Formalism

The rest of our animations are animated plots of our evolution variables. In order to understand them, it helps to know a little about the formalism we have used.

We simulate the early universe using a constant equation of state perfect fluid. For the purpose of these simulations, we take $w = 1/3$, corresponding to a radiation fluid. We use A as a comoving radius, and define a dimensionless comoving radius $\bar{A} = A/R_H$, where R_H is the horizon radius at the time of the initial data. The Misner-Sharp formalism uses a cosmic time variable defined by appropriate gauge conditions, and we evolve forwards using dimensionless time ξ defined by $t = t_0 e^{\xi}$.

The Misner-Sharp formalism evolves three quantities forwards in time: the areal radius $R(A,t)$, which is a gauge variable, the fluid coordinate velocity $U(A,t)$, and the mass

$$m(A,t) = 4\pi \int_0^A \rho R^2 \partial_A R dA \tag{212}$$

which can be thought of as the mass enclosed in the comoving radius A. The density ρ can be computed from m and R. For a number of reasons, it makes more sense to evolve quantities normalized by the values of the background cosmology, and so we define dimensionless tilded quantities $\tilde{R}$, $\tilde{U}$, $\tilde{m}$ and $\tilde{\rho}$ as

$$R = aA\tilde{R} = R_b\tilde{R} \tag{213a}$$

$$U = HR\tilde{U} \tag{213b}$$

$$m = \frac{4\pi}{3}\rho_b R^3 \tilde{m} \tag{213c}$$

$$\rho = \rho_b \tilde{\rho} \tag{213d}$$

where ρ_b is the background (asymptotic) energy density. When evolving FRW, all tilded quantities are unity. It turns out that the initial background density ρ_0 scales out of all the equations, and that all that is needed to specify initial data that consists only of a growing mode is an initial function for $\tilde{m} = \tilde{m}_0$, from which initial data for $\tilde{R}_0$ and $\tilde{U}_0$ can be computed.

For the next six animations, we demonstrate the evolution of two Gaussian initial profiles for $\tilde{m}_0$, taken a little over and under the threshold for black hole formation. In particular, we take

$$\tilde{m}_0 = 1 + \kappa e^{-A^2/2\sigma^2} \tag{214}$$

with $\sigma = 2R_H$ and $\kappa_1 = 0.173$, $\kappa_2 = 0.175$[13]. We take our domain to be $A_{max} = 20R_H$. In the animations, the teal curve represents κ_1, which doesn't form a black hole, and the purple curve represents κ_2, which does.

[13] Our first animation is of the energy density from the evolution using κ_2.

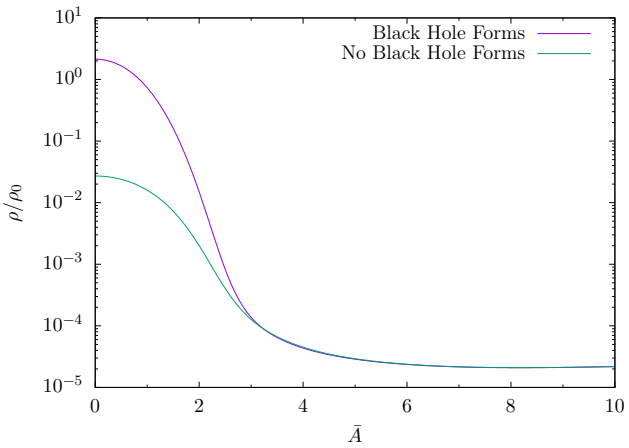

Figure 8. Density profile ρ/ρ_0 as a function of comoving radius just after black hole formation. Change to $\tilde{R}$

After a black hole has formed, the singularity at its center rapidly forms, we can no longer evolve the simulation, and the purple curve in the animations vanishes. All of the plots displayed here are still frames from the animations, taken shortly after black hole formation.

The animation "Density Profile" plots the density ρ/ρ_0 as a function of comoving radius $\bar{A}$. The initial part of the animation looks incredibly flat, and shows the dilution of energy density due to the expansion of the universe. After some time, mass begins to accumulate near the origin and the black hole formation process begins. The density near the forming black hole remains many times higher than the background density, which continues to decay. As the purple curve forms a black hole, the density at the origin grows without bound. Our numerical simulation breaks down just before the singularity forms, and the purple curve vanishes at this point. When the teal curve fails to form a black hole, the extra energy is blasted out in a spherical wave. Note that the asymptotic (background) energy density drops at a constant rate, which occurs because we use a logarithmic time coordinate. The density profiles just after black hole formation are shown in Fig. 8.

The next animation "Density Perturbation (Comoving Radius)" shows the density profile relative to the background density, which scales out the dilution due to the expansion of the universe. We see that the purple curve continues to increase in relative density until the black hole actually forms, while the teal curve reaches a peak of around a thousand times the background density before coming crashing down and releasing an outwards-moving density wave. The pressure when the teal curve peaks pushes the material out so rapidly that there is a strong rarefaction at the origin. The outgoing wave eventually forms a shockwave, which travels much faster than the speed of sound in the fluid. A still frame is shown in Fig. 9.

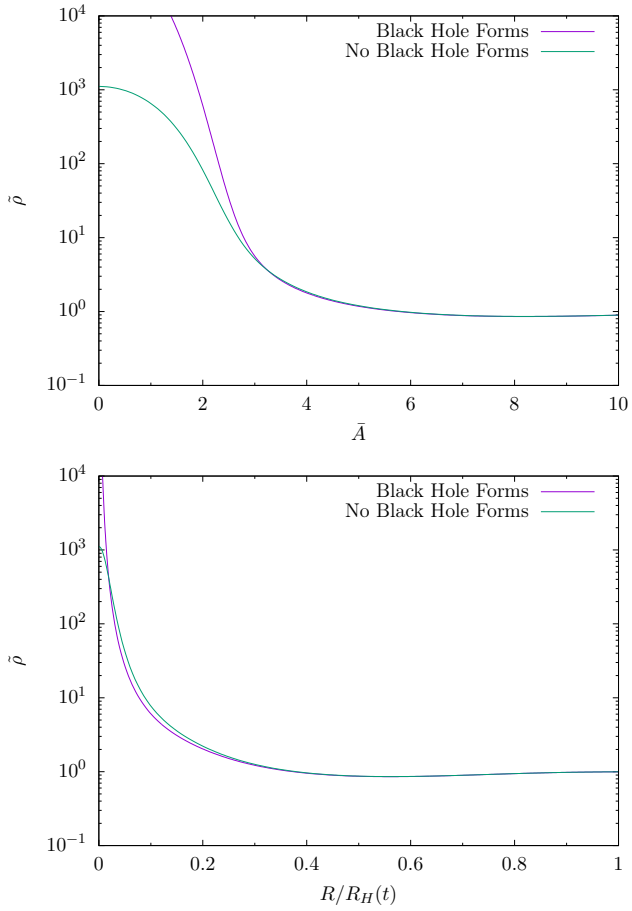

Figure 9. Density profile $\tilde{\rho}$ as a function of comoving radius (above) and areal radius (below) just after black hole formation. The below curve has its x-axis scaled such that the horizon scale is at 1.

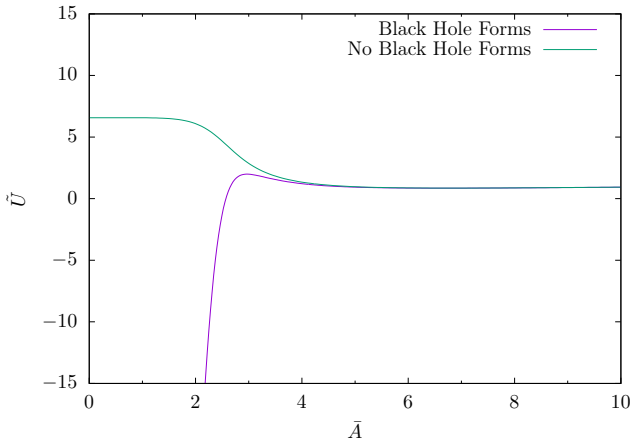

Figure 10. Velocity perturbation as a function of comoving radius just after black hole formation.

The fourth animation "Density Perturbation (Physical Radius)" again shows the density profile relative to the background density, but this time plots it as a function of physical radius normalized by the horizon radius at the time (computed based on the background cosmology). Thus, $R/R_H = 1$ shows what is happening at the horizon scale at that time. Since the horizon grows with time, the horizontal scale corresponds to larger and larger physical distances as time progresses. We can clearly see when the perturbation has entered the horizon (when $\tilde{\rho}$ drops below unity at $R/R_H = 1$). Note that at the very end, the horizon scale grows larger than our domain of evolution, and so the outermost point we have data for recedes towards the left. It is interesting to compare the two plots in Fig. 9; by looking at features in these plots, we can see the difference between comoving radius and physical radius. In particular, the inner radius has been squashed somewhat, while the region where the teal curve lies above the purple curve has been extended.

The fifth video "Velocity Perturbation" shows the normalized velocity perturbation as a function of comoving radius. Normalized velocities less than one are expanding slower than the Hubble rate, while negative velocities are moving in the opposite direction of the Hubble flow, attracted into the growing overdensity. Initially, the velocity is essentially unity everywhere, indicating that matter is moving with the Hubble flow. We can clearly see when matter begins to fall towards the central overdensity. Eventually, the pressure of the overdensity dominates over the gravitational pull for the teal curve, and the velocity rises very sharply, explosively sending out a wave of matter (or photons, as the case may be). For the purple curve, the velocity continues to grow negative as matter continues to fall into the overdensity, until a black hole is formed. It is interesting to note a small apparent outflow ($\tilde{U} > 1$) from the black hole-forming region. This turns out to be a coordinate velocity effect; as the relationship between physical velocity and coordinate velocity has become rather stretched in this vicinity, matter is still actually flowing inwards. The normalized velocity for the teal curve returns very rapidly to unity, despite being largely uninfluenced by the background cosmology. We believe that this is at least partly due to our gauge condition. A still frame can be seen in Fig. 10.

Animations 6 and 7 ("Black Hole Detection (Comoving Radius)" and "Black Hole Detection (Physical Radius)") demonstrate the evolution of the quantity $2m/R$ as a function of radius. The black hole formation condition is $2m/R = 1$ (with $G = c = 1$; Eq. (52)), which signifies the formation of an apparent horizon (which must be contained within an event horizon). We see that after the purple curve crosses the yellow line, a singularity rapidly forms, and we cannot evolve it any further (the purple curve vanishes). There is a second condition for a black hole to form, namely that $\tilde{U}$ must be negative at that point, which is why the curves can cross the yellow line at large radii without issue (the velocity there is roughly the Hubble flow, or $\tilde{U} \sim 1$). Still frames are shown in Fig. 11. Again, the difference between comoving coordinates and

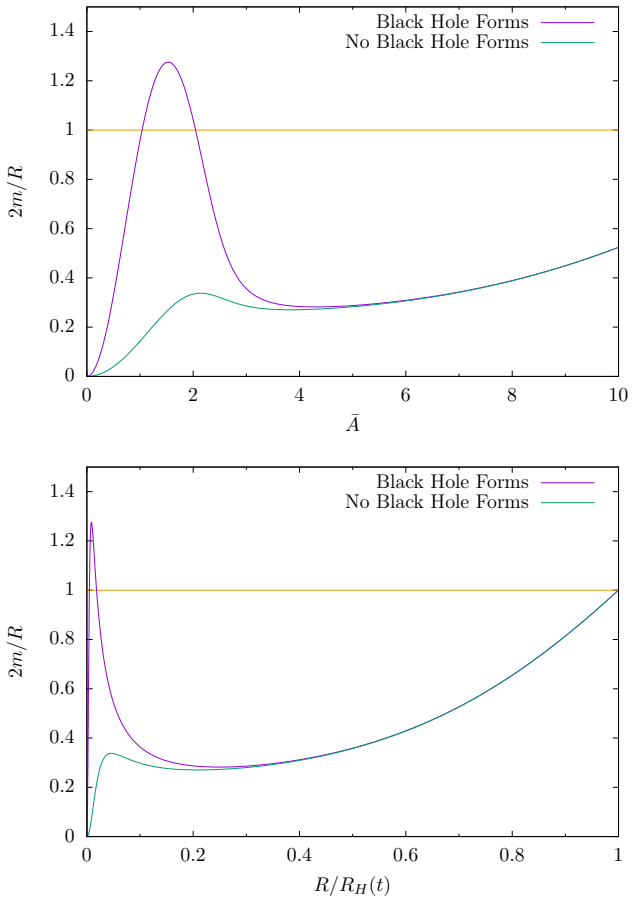

Figure 11. Above: Plot of the black hole detection condition as a function of comoving radius. Below: The same plot, but as a function of normalized areal radius (such that 1 is the horizon scale at that time). A horizon has formed when a curve lies above the yellow line and $\tilde{U} < 0$ (cf. Fig. 10).

physical radius can be seen in the comparison between these two plots.

C. Hernandez-Misner Formalism

The Misner-Sharp formalism cannot evolve much past the formation of a black hole, due to the formation of a singularity. The Hernandez-Misner formalism aims to overcome this shortcoming by using a null time coordinate u. Data on a slice of constant u represents what an observer at the outer boundary of the computational domain sees at that instant, retarded by the distance that the light needs to travel to get to them. As no null rays ever leave an event horizon, a black hole never forms from the perspective of this observer. In particular, the lapse near the formation of a black hole approaches zero, which indicates that evolution is essentially frozen. Even though a black hole never forms, one can extract information about the black hole by looking at where the

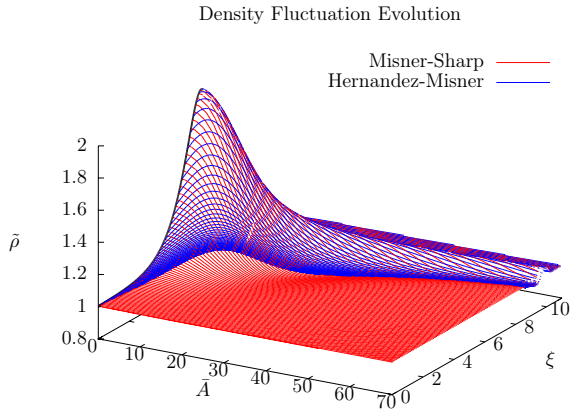

Figure 12. A plot of the density perturbation $\tilde{\rho}$ as a function of $\bar{A}$ and ξ in both the Misner-Sharp (red) and Misner-Hernandez (blue) coordinate systems.

lapse becomes nonzero again.

The Hernandez-Misner formalism evolves the same variables as the Misner-Sharp formalism, just using a different coordinate system. The initial data for these variables has to come from a Misner-Sharp evolution, as constructing initial data on a null slice is somewhat unusual. A strong test of one's code is to check to see that the evolution of a system is the same in the two different coordinate systems. This comparison is demonstrated in the eighth animation, "Two Coordinate Systems".

In this animation, we show a three-dimensional plot with comoving radius $\bar{A}$ on the x-axis, logarithmic time ξ on the y-axis, and density perturbation $\tilde{\rho}$ on the z-axis for an evolution that did not form a black hole. The red lines show timesteps from the Misner-Sharp evolution, where each time step is at constant ξ. The blue lines show timesteps from the Hernandez-Misner evolution, where each timestep is a null ray in the spacetime. The excellent agreement of the two surfaces shows that the evolution is in agreement between the two coordinate systems, including at the boundaries. A still frame from this animation is shown in Fig. 12.

The rest of our animations are of the same purple black-hole-forming data that we showed in the Misner-Sharp animations above.

Our next animation, "Density Profile (Null Slicing)", is of the density profile in the Hernandez-Misner coordinates, plotting the physical density ρ as a function of areal radius. We see that the density profile forms a large bump near the origin, as shown in Fig. 13. However, this bump is very much frozen in time by the vanishing lapse. In the Misner-Sharp coordinates, the density grows without bound at the origin; here, because we do not pierce the event horizon, it merely reaches a large density and stays fixed. As the evolution progresses, we see the energy

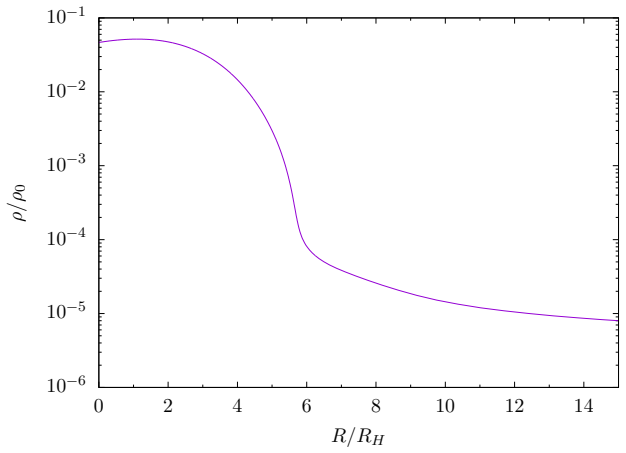

Figure 13. A plot of the physical density ρ as a function of areal radius. The large bump to the left has essentially been frozen in place. Together, the energy contained in this frozen bump constitutes the mass of the black hole.

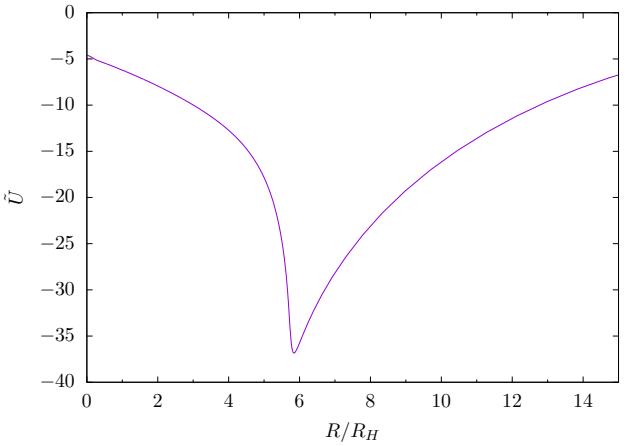

Figure 14. This plot shows a frame from an animation of $\tilde{U}$ as a function of areal radius, late in the formation of the black hole. As $\tilde{U}$ is always negative, matter is sharply falling into the black hole.

density outside the black hole continues to fall off with cosmic expansion, though some matter accretes onto the black hole and freezes. Note that due to the null slicing, points on the curve at larger radius correspond to later times, and thus more expansion has occurred, decreasing the energy density.

The animation "Velocity Perturbation (Null Slicing)" of the normalized velocity perturbation $\tilde{U}$ as a function of areal radius shows the formation of a huge negative spike when the black hole forms. Figure 14 shows a frame from late in the animation. We see that all matter is falling sharply inwards (recall that $\tilde{U} = 1$ is the Hubble flow). The animation also exhibits the freezing of the lapse. Starting from the origin, a trail of "frozen" velocity profile creeps outwards.

Our final animation, "Lapse in the Null Slicing", is that of the lapse as a function of areal radius. We do not include a still frame plot here, as the animation is simply an animated version of Fig. 3. The animation clearly shows the lapse rapidly vanishing, which freezes the evolution of all variables.

VIII. CONCLUSIONS

We have presented a comprehensive formalism for investigating primordial black hole formation in full general relativity. The basic idea is to construct an initial density profile and evolve it forwards in time using a standard time-slicing until either a black hole forms or the overdensity disperses. If a black hole forms, a second formalism that avoids the formation of a singularity is used to continue the evolution and compute the mass of the resulting black hole.

The foundation of the approach is the Misner-Sharp formalism, which we have adapted to cosmological applications. We paid special attention to the outer boundary, where we constructed a non-reflecting boundary condition. For extracting information about black holes that form, we turned to the Hernandez-Misner formalism. Here, we adapted the system of equations to use variables more suited to cosmological and numerical evolution.

The issue of initial conditions was explored in detail, where we identified an expansion in two small parameters, and explicitly constructed initial conditions consisting only of the linear cosmological growing mode to second order, based on a single function δ_{m0}. The regime of validity of the expansion was investigated, including both perturbative convergence and physical constraints. We related these initial conditions to a variety of approaches in the literature, including Carr's fractional mass excess, Polnarev's initial curvature perturbation, Bardeen gauge invariant variables, and physical perturbation profiles at the end of inflation.

The approach that has been developed here builds upon numerous other approaches in the literature. Most importantly, various ideas from the literature have been combined to form a clear and comprehensive picture. Numerically, there are numerous benefits to the enhancements we have incorporated, including completely stable cosmological background evolution, increased computational efficiency, and increased numerical accuracy. Theoretically, we have investigated initial conditions in unprecedented detail, constructed a rigorous connection to inflation, introduced appropriate cosmological boundary conditions, and clarified the role of the initial curvature perturbation within this formalism.

In addition to describing the formalism, we have constructed a number of animations to describe what happens in primordial black hole formation and near misses. We hope that these animations will help spur interest in the subject, and provide a visual interpretation of what

actually happens in primordial black hole formation.

We plan to use the formalism developed here to investigate properties of initial profiles that give rise to black holes and to quantify the resulting black hole masses that are produced. In the long term, we hope to run Monte Carlo simulations from inflationary initial profiles to identify the number density and mass spectrum of primordial black holes formed from different models of inflation.

ACKNOWLEDGMENTS

We thank Mark Hertzberg, Evangelos Sfakianakis, Alan Guth, Curran Muhlberger, Scott Hughes, Geoffrey Lovelace and Gerard Pascual-Lopez for helpful discussions. This work is supported in part by the U.S. Department of Energy under grant Contract Number DE-SC00012567, and in part by MIT's Undergraduate Research Opportunities Program.

Appendix A: Stress-Energy Tensor

In this appendix, we derive the stress-energy tensor for a spherically symmetric fluid, based on a statistical description of the system. This reproduces standard derivations, and is included for completeness.

The description of a particle in a generic space-time is given by its position and momentum $\{x^\alpha(\lambda), p^\alpha(\lambda)\}$, where an affine parameter λ is employed. The momentum is related to the position through

$$p^\alpha \equiv \frac{dx^\alpha}{d\lambda}\left[= m\frac{dx^\alpha}{d\tau}\right] \tag{A1}$$

where the second equivalence is only defined for massive particles of mass m. A particle's momentum obeys the mass shell equation,

$$g^{\alpha\beta}p_\alpha p_\beta = -m^2\,. \tag{A2}$$

Note that given the spatial components of a particle's four-momentum, this constraint determines the four-momentum time component, and thus only three of the four components of momentum are independent.

Analogously to the definition in Special Relativity, we definite the *number density of particles in phase space* $\mathcal{N}$ to be the function which describes the number of particles per unit volume in both position and momentum space. When integrated over any space-like hypersurface Σ and set of momenta $\mathcal{R}$, this yields the total number of particles in Σ and $\mathcal{R}$.

$$N = \int_\Sigma d^3\Sigma_\alpha(x^\beta)\int_\mathcal{R} d\mu(p_\beta)p^\alpha\mathcal{N}(x^\beta,p_\beta) \tag{A3}$$

Here, $p^\alpha d\Sigma_\alpha(x^\beta)$ and $d\mu(p_\beta)$ are the invariant volume measures of Σ and $\mathcal{R}$ respectively. The 3-dimensional volume element $d\Sigma_\alpha(x^\beta)$ takes the form,

$$d\Sigma_\alpha(x^\beta) = \epsilon_{\mu\nu\sigma\alpha}\frac{\partial x^\mu}{\partial a}\frac{\partial x^\nu}{\partial b}\frac{\partial x^\sigma}{\partial c}dadbdc \tag{A4}$$

where $\epsilon_{\mu\nu\sigma\alpha}$ is the antisymmetric tensor with $\epsilon_{0123} = +1$, and we have parameterized Σ by (a,b,c) so that $x^\alpha = x^\alpha(a,b,c)$. Since Σ is a 3-dimensional hypersurface in a 4-dimensional manifold, its volume element is a vector pointing along the direction normal to it. In order to construct a scalar from $d\Sigma_\alpha(x^\beta)$ we must take its inner product with another four-vector. The only other true four-vector available in a statistical picture is the four-momentum p^α, which we use to construct the invariant volume.

The invariant momentum volume element is

$$d\mu(p_\beta) = 2\delta\left(p^\beta p_\beta + m^2\right)\Theta(p^0)\frac{d^4p}{\sqrt{-g}}\,. \tag{A5}$$

The delta function guarantees the momenta obey the constraint A2, and the step-function Θ picks out the positive energy solution. The factor of two arises from the fact that momentum is squared in the delta function. Note that the infinitesimals dp refer to momenta with lowered index (this arises because p_α is the conjugate momentum to x^α).

Note that in Minkowski spacetime on a constant time slice, we have $d\Sigma_\alpha(x^\beta) = (1,\vec{0})d^3x$, $p^\alpha = (E,\vec{p})$, and $d\mu(p^\beta) = \frac{1}{E}d^3p$, so A3 reduces to

$$N = \int_\Sigma d^3x\int_\mathcal{R} d^3p\,\mathcal{N}(t,\vec{x},\vec{p}) \tag{A6}$$

as expected, where we have integrated over the delta function in momentum space. A number density per volume in space can be obtained by simply not integrating over the spatial hypersurface.

We can take different moments of the number density $\mathcal{N}$ by multiplying it by p^α and integrating over momentum space. In particular, we can define the *stress-energy tensor* by the integral

$$T^{\alpha\beta}(x^\nu) \equiv \int d\mu(p_\nu)p^\alpha p^\beta\mathcal{N}(x^\nu,p_\nu)\,. \tag{A7}$$

Ignoring normalization, this is the only rank two tensor which we can construct from the invariants $\mathcal{N}$, p^μ, and $d\mu(p_\nu)$ that is linear in $\mathcal{N}$. One can be readily check that this object agrees with the usual stress-energy tensor by transforming to a local Lorentz frame.

Let us now construct the stress-energy tensor in spherical coordinates. In order to compute the stress-energy tensor, we need to integrate over all possible momenta at a given position in space $x^i = (r,\theta,\phi)$. To facilitate this, we construct an orthonormal Cartesian basis at x^i, oriented such that the x direction aligns with $\hat{r}$, the y direction aligns with $\hat{\theta}$, and the z direction aligns with $\hat{\phi}$. We can then describe momenta at that point in space

through the components (p^x, p^y, p^z) in the orthonormal basis. For the metric described in Eq. (4), these components are related to the momenta $p^\mu = (p^0, p^r, p^\theta, p^\phi)$ by

$$p^r = \frac{p^x}{e^{\lambda/2}} \tag{A8a}$$

$$p^\theta = \frac{p^y}{R} \tag{A8b}$$

$$p^\phi = \frac{p^z}{R\sin\theta}\,. \tag{A8c}$$

We now write the components of the momentum in the orthonormal basis in spherical polar coordinates defined by

$$(p^x, p^y, p^z) = (p\cos\Theta, p\sin\Theta\cos\Phi, p\sin\Theta\sin\Phi)\,. \tag{A9}$$

eq:app:porthonormal

Here, Θ denotes the angle away from the radial (x) axis, while Φ is the azimuthal angle about the radial direction, and $p^2 = (p^x)^2 + (p^y)^2 + (p^z)^2$.

We can now construct p_r, p_θ and p_ϕ in terms of p, Θ and Φ. Begin by noting that $p_x = p^x$, thanks to the orthonormal basis. We can then construct the following relationships.

$$p_r = e^{\lambda/2}p_x = e^{\lambda/2}p\cos\Theta \tag{A10a}$$

$$p_\theta = Rp_y = Rp\sin\Theta\cos\Phi \tag{A10b}$$

$$p_\phi = R\sin\theta p_z = Rp\sin\Theta\sin\Phi \tag{A10c}$$

The volume element $d^4p/\sqrt{-g}$ on momentum space then becomes the following.

$$\begin{aligned}\frac{d^4p}{\sqrt{-g}} &= \frac{1}{e^\phi e^{\lambda/2}R^2\sin\theta}dp_0\,dp_r\,dp_\theta\,dp_\phi \\ &= e^{-\phi}dp_0\,dp_x\,dp_y\,dp_z \\ &= e^{-\phi}dp_0\,p^2\,\sin\Theta\,dp\,d\Theta\,d\Phi\end{aligned} \tag{A11}$$

The range of p is from 0 to ∞, while $0 \le \Theta \le \pi$ and $0 \le \Phi < 2\pi$. The complete integration measure on momentum space then becomes

$$d\mu(p^\nu) = 2\delta\left(-\frac{p_0^2}{e^{2\phi}} + p^2\right)\Theta(p^0)\frac{dp_0}{e^\phi}\,p^2\,\sin\Theta\,dp\,d\Theta\,d\Phi \tag{A12}$$

eq:intmes

where we take $m = 0$.

We now calculate the stress-energy tensor. Inserting the integration measure (A12) into Eq. (A7) and integrating over the delta function, we arrive at

$$T^{\alpha\beta} = \int p^3\,\sin\Theta\,dp\,d\Theta\,d\Phi\,n^\alpha n^\beta\mathcal{N} \tag{A13}$$

eq:app:stresspartway

where we have defined

$$n^\alpha = p^\alpha/p = \left(e^{-\phi}, \frac{\cos\Theta}{e^{\lambda/2}}, \frac{\sin\Theta\cos\Phi}{R}, \frac{\sin\Theta\sin\Phi}{R\sin\theta}\right). \tag{A14}$$

In order for the distribution to be spherically symmetric, we require it to be a function of

$$\mathcal{N}(x^\alpha, p_\alpha) = \mathcal{N}(t, r, p, \Theta) \tag{A15}$$

only, where $\cos\Theta$ is related to the rotationally invariant dot product $x^i p_i$. Note that $p = \sqrt{g^{ij}p_i p_j}$ is also rotationally invariant.

Evaluating the integrals in Eq. (A13) over Θ and Φ component by component, we find

$$T^{tt} = 2\pi e^{-2\phi}\int f\,d\zeta \tag{A16a}$$

$$T^{tr} = 2\pi e^{-\phi-\lambda/2}\int \zeta f\,d\zeta \tag{A16b}$$

$$T^{rr} = 2\pi e^{-\lambda}\int \zeta^2 f\,d\zeta \tag{A16c}$$

$$T^{\theta\theta} = \frac{\pi}{R^2}\int (1-\zeta^2) f\,d\zeta \tag{A16d}$$

$$T^{\phi\phi} = \frac{\pi}{R^2\sin^2\theta}\int (1-\zeta^2) f\,d\mu \tag{A16e}$$

with all other components vanishing, where we use $\zeta = \cos\Theta$ and define

$$f(t, r, \zeta) = \int p^3\,\mathcal{N}\,dp\,. \tag{A17}$$

Each of these integrals involves different moments of the function f with respect to the variable ζ.

If we assume that the particles in the spacetime in question are in thermal equilibrium, then at a given point in space, particles have equal probability to be going in any direction, and so f cannot depend on ζ. Under this assumption, the off-diagonal component vanishes, and if we set

$$u^\alpha = (e^{-\phi}, 0, 0, 0) \tag{A18a}$$

$$\rho = 2\pi\int f\,d\zeta \tag{A18b}$$

$$P = \frac{\rho}{3} \tag{A18c}$$

then we can write $T^{\alpha\beta}$ as

$$T^{\alpha\beta} = Pg^{\alpha\beta} + u^\alpha u^\beta(\rho + P) \tag{A19}$$

which is a perfect fluid in comoving coordinates, and the desired result. Note that this also yields that the equation of state of radiation is $w = 1/3$.

One might ask how non-interacting radiation (photons and neutrinos) can yield a fluid description. The key assumption that facilitated this was that of thermal equilibrium. So long as there are other species present in the universe to scatter radiation efficiently enough to maintain thermal equilibrium, then the radiation bath behaves like a fluid. When neutrinos decouple from the bath and begin to freely stream, then the thermal equilibrium assumption will no longer hold, and the stress-energy tensor

will develop an off-diagonal T^{tr} component. At this stage, the photon bath may still be described by a perfect fluid, but the evolution of the neutrino species will have to be described by the full Boltzmann equation. Such a description is beyond the scope of the formalism described in this paper.

Appendix B: Connection to Cosmological Perturbation Theory

In this appendix, we connect the formalism developed in this paper to standard cosmological perturbation theory.

1. Standard Cosmological Perturbation Theory

We consider the perturbed FRW metric

$$\begin{aligned} ds^2 = & -(1+2\phi)dt^2 + 2a\tilde{\nabla}_i B\, dx^i dt \\ & + a^2\left[(1-2\psi)\tilde{g}_{ij} + 2\tilde{\nabla}_i\tilde{\nabla}_j E\right] dx^i dx^j \end{aligned} \tag{B1}$$

eq:whollyperturbed

where $\tilde{g}_{ij}$ is the background flat, time-independent three-dimensional metric on space, and $\tilde{\nabla}_i$ are covariant derivatives associated with this metric (we raise and lower indices on $\tilde{\nabla}_i$ with $\tilde{g}_{ij}$). We include only scalar perturbations, as that is sufficient for our purposes. Consider the transformation

$$x^\mu \to x^\mu + \xi^\mu(t, x^i) \tag{B2}$$

with

$$\xi^0 = T, \qquad \xi^i = L^i = \tilde{\nabla}^i L\,. \tag{B3}$$

Under this transformation,

$$\delta g_{\mu\nu} \to \delta g_{\mu\nu} - \mathcal{L}_\xi \bar{g}_{\mu\nu} \tag{B4}$$

where $\bar{g}_{\mu\nu}$ is the background metric, and the Lie derivative is given by

$$\mathcal{L}_\xi \bar{g}_{\mu\nu} = \xi^\lambda \partial_\lambda \bar{g}_{\mu\nu} + \partial_\mu \xi^\lambda \bar{g}_{\lambda\nu} + \partial_\nu \xi^\lambda \bar{g}_{\mu\lambda}\,. \tag{B5}$$

Evaluating the Lie derivative yields the following, where dots represent time derivatives.

$$\mathcal{L}_\xi \bar{g}_{tt} = -2\dot{T} \tag{B6}$$

$$\mathcal{L}_\xi \bar{g}_{ti} = \tilde{\nabla}_i(a^2\dot{L} - T) \tag{B7}$$

$$\mathcal{L}_\xi \bar{g}_{ij} = 2a^2(TH\tilde{g}_{ij} + \tilde{\nabla}_i\tilde{\nabla}_j L) \tag{B8}$$

The metric scalars in Eq. (B1) then transform in the following manner.

$$\phi \to \phi - \dot{T} \tag{B9}$$

$$B \to B + \frac{T}{a} - a\dot{L} \tag{B10}$$

$$\psi \to \psi + HT \tag{B11}$$

$$E \to E - L \tag{B12}$$

The Bardeen gauge invariant potentials [56] are the following combinations of these potentials.

$$\Phi = \phi + \partial_t(aB - a^2\dot{E}) \tag{B13}$$

eq:bardeen

$$\Psi = \psi - H(aB - a^2\dot{E}) \tag{B14}$$

We should also consider how the stress-energy tensor transforms under a gauge transformation. Let us split the stress-energy tensor into a background and perturbed component as

$$T^\mu{}_\nu = \bar{T}^\mu{}_\nu + \delta T^\mu{}_\nu \tag{B15}$$

where

$$\bar{T}^\mu{}_\nu = (\rho_b + P_b)u_b^\mu u_{b\nu} + P_b\delta^\mu_\nu \tag{B16}$$

with u_b^μ being the background value of u^μ. Let us write the perturbed stress-energy tensor as

$$\begin{aligned} \delta T^\mu{}_\nu = & (\delta\rho + \delta P)u_b^\mu u_{b\nu} + (\rho_b + P_b)(\delta u^\mu u_{b\nu} + u_b^\mu \delta u_\nu) \\ & + \delta P\delta^\mu_\nu + \Pi^\mu{}_\nu \end{aligned} \tag{B17}$$

where we again work only with scalar perturbations. We decompose u^μ as

$$u^\mu = [1-\phi, \tilde{\nabla}^i v/a] \tag{B18}$$

$$u_\mu = [-(1+\phi), a\tilde{\nabla}_i(v+B)] \tag{B19}$$

and use

$$\Pi^0{}_\nu = \Pi^\mu{}_0 = 0 \tag{B20}$$

$$\Pi^i{}_j = \left(\tilde{\nabla}^i\tilde{\nabla}_j - \frac{\delta^i_j}{3}\tilde{\nabla}^2\right)\Pi\,. \tag{B21}$$

The components of the stress-energy tensor are then

$$T^0{}_0 = -(\rho_b + \delta\rho) \tag{B22}$$

$$T^i{}_0 = -(\rho_b + P_b)\tilde{\nabla}^i v/a \tag{B23}$$

$$T^0{}_j = a(\rho_b + P_b)\tilde{\nabla}_i(v+B) \tag{B24}$$

$$T^i{}_j = (P_b + \delta P)\delta^i_j + \Pi^i{}_j\,. \tag{B25}$$

Under a gauge transformation, the stress-energy tensor transforms as

$$\delta T^\mu{}_\nu \to \delta T^\mu{}_\nu - \mathcal{L}_\xi \bar{T}^\mu{}_\nu \tag{B26}$$

where the Lie derivative is given by

$$\mathcal{L}_\xi \bar{T}^\mu{}_\nu = \xi^\lambda\partial_\lambda \bar{T}^\mu{}_\nu + \partial_\nu\xi^\lambda \bar{T}^\mu{}_\lambda - \partial_\lambda\xi^\mu \bar{T}^\lambda{}_\nu\,. \tag{B27}$$

Evaluating the Lie derivatives for ξ^μ defined above yields the following.

$$\mathcal{L}_\xi \bar{T}^0{}_0 = -T\dot{\rho}_b \tag{B28}$$

$$\mathcal{L}_\xi \bar{T}^i{}_0 = (\rho_b + P_b)\tilde{\nabla}^i\dot{L} \tag{B29}$$

$$\mathcal{L}_\xi \bar{T}^0{}_j = -(\rho_b + P_b)\tilde{\nabla}_j T \tag{B30}$$

$$\mathcal{L}_\xi \bar{T}^i{}_j = T\dot{P}_b\delta^i_j \tag{B31}$$

The scalars in the stress-energy tensor then transform in the following manner.

$$\delta\rho \to \delta\rho - T\dot{\rho}_b \tag{B32}$$

$$\delta P \to \delta P - T\dot{P}_b \tag{B33}$$

$$v \to v + a\dot{L} \tag{B34}$$

$$\Pi \to \Pi \tag{B35}$$

A variety of gauge invariant quantities can be constructed for the matter perturbations. We focus on two of them. The first is the comoving density contrast Δ, defined by

$$\rho_b \Delta = \delta\rho + a\dot{\rho}_b(v + B)\,. \tag{B36}$$

The second, which we shall refer to as the gauge invariant velocity perturbation (as we are unaware of any standard name), is given by

$$V = v + a\dot{E}\,. \tag{B37}$$

2. Connection to Misner-Sharp Formalism

We now cast the Misner-Sharp metric (4) into the above language. Writing

$$R = aR_H\tilde{R} = aA(1 + \delta_R) \tag{B38}$$

$$e^{\lambda/2} = \frac{\partial_A R}{\Gamma} = a\frac{1 + \delta_R + A\partial_A\delta_R}{1 + \delta_\Gamma} \tag{B39}$$

where

$$\delta_\Gamma = e^{2(\alpha-1)\xi}\bar{A}^2\left(\delta_U - \frac{1}{2}\delta_m\right) \tag{B40}$$

eq:app:deltag

and expanding the metric to first order in δ_R, δ_Γ and ϕ, we obtain the following.

$$\begin{aligned} ds^2 = &-(1 + 2\phi)dt^2 + a^2(1 + 2\delta_R)(dA^2 + A^2 d\Omega^2) \\ &+ a^2(2A\partial_A\delta_R - 2\delta_\Gamma)dA^2 \end{aligned} \tag{B41}$$

eq:pertmetric

This metric contains three scalar perturbations, as expected in a comoving gauge. No vector or tensor components are present.

Looking back at the metric in Eq. (B1), let us take the metric $\tilde{g}_{ij}$ to be the metric in spherical polar coordinates with radius A. We evaluate the quantity

$$\tilde{\nabla}_i\tilde{\nabla}_j E dx^i dx^j = \partial_A^2 E dA^2 + A\partial_A E d\Omega^2\,. \tag{B42}$$

Letting ϕ, ψ and E become functions of A and t alone, we can identify the coefficients in Eqs. (B1) and (B41) to obtain

$$\delta_R = -\psi + \frac{\partial_A E}{A} \tag{B43}$$

$$\delta_\Gamma = -A\partial_A\psi\,. \tag{B44}$$

The quantity ϕ is the same in both descriptions, and we have $B = 0$.

We now relate our quantities to the Bardeen potentials (B13). In order to do so, we need to compute $\dot{E}$, which in turn requires $\dot{\psi}$. We thus start with ψ.

$$\psi = \int_{\bar{A}}^{\infty}\frac{\delta_\Gamma}{\bar{A}'}d\bar{A}' \tag{B45}$$

The limits of integration are set by the requirement that all perturbations vanish at infinity. In order to compute $\dot{\psi}$, we first compute

$$\partial_\xi\psi = \int_{\bar{A}}^{\infty}\frac{\partial_\xi\delta_\Gamma}{\bar{A}'}d\bar{A}' \tag{B46}$$

where

$$\partial_\xi\delta_\Gamma = -\bar{A}\frac{3w\alpha^2}{2}\partial_{\bar{A}}\delta_\rho \tag{B47}$$

and we have used Eq. (57d) to simplify this expression. We then have

$$\dot{\psi} = \frac{3w\alpha}{2}H\delta_\rho\,. \tag{B48}$$

Next, we look towards E. Taking our expression for δ_R and integrating as we did for ψ, we obtain

$$E = -R_H^2\int_{\bar{A}}^{\infty}\bar{A}'(\psi + \delta_R)d\bar{A}'\,. \tag{B49}$$

We then compute $\partial_\xi E$ as a step towards $\dot{E}$, using Eqs. (55a) and (55b) to simplify the result.

$$\dot{E} = -HR_H^2\int_{\bar{A}}^{\infty}\bar{A}'\delta_U d\bar{A}' \tag{B50}$$

The first gauge invariant variable is then

$$\Psi = -\frac{1}{2}e^{2(\alpha-1)\xi}\int_{\bar{A}}^{\infty}\bar{A}'\delta_m d\bar{A}' \tag{B51}$$

where we use the definition of δ_Γ (B40).

For the second gauge invariant variable, we need $\partial_t(a^2\dot{E})$. As before, it is simplest to calculate $\partial_\xi(a^2\dot{E})$ and then convert the result. We find

$$\partial_t(a^2\dot{E}) = \frac{1}{2}e^{2(\alpha-1)\xi}\int_{\bar{A}}^{\infty}\bar{A}'\,\delta_m d\bar{A}' - \frac{3w\alpha}{2}\delta_\rho, \tag{B52}$$

where we've used Eq. (55e) to substitute for $\partial_\xi\delta_U$. The second gauge invariant variable is then

$$\Phi = -\frac{1}{2}e^{2(\alpha-1)\xi}\int_{\bar{A}}^{\infty}\bar{A}'\,\delta_m d\bar{A}' = \Psi \tag{B53}$$

where we substitute ϕ from Eq. (55a). We could have anticipated this result; a perfect fluid has no anisotropic shear stress, and so the two Newtonian potentials, and thus the Bardeen gauge invariant variables, are the same.

The gauge invariant density contrast is simply $\Delta = \delta_\rho$, thanks to the comoving gauge and diagonal metric. The gauge invariant velocity perturbation is

$$V = a\dot{E} = -R_H e^{(\alpha-1)\xi}\int_{\bar{A}}^{\infty}\bar{A}'\delta_U d\bar{A}'\,. \tag{B54}$$

[1] A. H. Guth, "The Inflationary Universe: A Possible Solution to the Horizon and Flatness Problems," *Phys.Rev.* **D23** (1981) 347–356.

[2] A. A. Starobinsky, "A New Type of Isotropic Cosmological Models Without Singularity," *Phys.Lett.* **B91** (1980) 99–102.

[3] J. Yokoyama, "Formation of primordial black holes in the inflationary universe," *Phys.Rept.* **307** (1998) 133–139.

[4] J. Yokoyama, "Formation of primordial black holes in inflationary cosmology," *Prog.Theor.Phys.Suppl.* **136** (1999) 338–352.

[5] S. Young, C. T. Byrnes, and M. Sasaki, "Calculating the mass spectrum of primordial black holes," arXiv:1405.7023 [gr-qc].

[6] J. Garcia-Bellido, A. D. Linde, and D. Wands, "Density perturbations and black hole formation in hybrid inflation," *Phys.Rev.* **D54** (1996) 6040–6058, arXiv:astro-ph/9605094 [astro-ph].

[7] K. A. Thompson, "Formation and evolution of primordial black holes after hybrid inflation," *eConf* **C041213** (2004) 1107, arXiv:astro-ph/0504606 [astro-ph].

[8] E. Bugaev and P. Klimai, "Formation of primordial black holes from non-Gaussian perturbations produced in a waterfall transition," *Phys.Rev.* **D85** (2012) 103504, arXiv:1112.5601 [astro-ph.CO].

[9] N. Duechting, "Supermassive black holes from primordial black hole seeds," *Phys.Rev.* **D70** (2004) 064015, arXiv:astro-ph/0406260 [astro-ph].

[10] F. Capela, M. Pshirkov, and P. Tinyakov, "Constraints on primordial black holes as dark matter candidates from capture by neutron stars," *Phys.Rev.* **D87** (2013) no. 12, 123524, arXiv:1301.4984 [astro-ph.CO].

[11] S. Hawking, "Black hole explosions," *Nature* **248** (1974) 30–31.

[12] Y. B. Zel'dovich and I. D. Novikov, "The Hypothesis of Cores Retarded during Expansion and the Hot Cosmological Model,"Soviet Ast. **10** (Feb., 1967) 602.

[13] S. Hawking, "Gravitationally collapsed objects of very low mass," MNRAS **152** (1971) 75.

[14] B. J. Carr and S. Hawking, "Black holes in the early Universe," *Mon.Not.Roy.Astron.Soc.* **168** (1974) 399–415.

[15] B. J. Carr, "The Primordial black hole mass spectrum," *Astrophys.J.* **201** (1975) 1–19.

[16] D. K. Nadezhin, I. D. Novikov, and A. G. Polnarev, "The hydrodynamics of primordial black hole formation,"Soviet Ast. **22** (Apr., 1978) 129–138.

[17] G. V. Bicknell and R. N. Henriksen, "Formation of primordial black holes,"ApJ **232** (Sept., 1979) 670–682.

[18] I. D. Novikov and A. G. Polnarev, "The Hydrodynamics of Primordial Black Hole Formation - Dependence on the Equation of State,"Soviet Ast. **24** (Apr., 1980) 147–151.

[19] M. Crawford and D. N. Schramm, "Spontaneous Generation of Density Perturbations in the Early Universe," *Nature* **298** (1982) 538–540.

[20] S. Hawking, "Black Holes From Cosmic Strings," *Phys.Lett.* **B231** (1989) 237.

[21] A. Polnarev and R. Zembowicz, "Formation of Primordial Black Holes by Cosmic Strings," *Phys.Rev.* **D43** (1991) 1106–1109.

[22] K. Jedamzik and J. C. Niemeyer, "Primordial black hole formation during first order phase transitions," *Phys.Rev.* **D59** (1999) 124014, arXiv:astro-ph/9901293 [astro-ph].

[23] A. M. Green, A. R. Liddle, K. A. Malik, and M. Sasaki, "A New calculation of the mass fraction of primordial black holes," *Phys.Rev.* **D70** (2004) 041502, arXiv:astro-ph/0403181 [astro-ph].

[24] A. M. Green and A. R. Liddle, "Constraints on the density perturbation spectrum from primordial black holes," *Phys.Rev.* **D56** (1997) 6166–6174, arXiv:astro-ph/9704251 [astro-ph].

[25] B. Carr, K. Kohri, Y. Sendouda, and J. Yokoyama, "New cosmological constraints on primordial black holes," *Phys.Rev.* **D81** (2010) 104019, arXiv:0912.5297 [astro-ph.CO].

[26] A. S. Josan, A. M. Green, and K. A. Malik, "Generalised constraints on the curvature perturbation from primordial black holes," *Phys.Rev.* **D79** (2009) 103520, arXiv:0903.3184 [astro-ph.CO].

[27] C. T. Byrnes, E. J. Copeland, and A. M. Green, "Primordial black holes as a tool for constraining non-Gaussianity," *Phys.Rev.* **D86** (2012) 043512, arXiv:1206.4188 [astro-ph.CO].

[28] K. Griest, A. M. Cieplak, and M. J. Lehner, "New Limits on Primordial Black Hole Dark Matter from an Analysis of Kepler Source Microlensing Data," *Phys.Rev.Lett.* **111** (2013) 181302, arXiv:1307.5798 [astro-ph.CO].

[29] B. Carr, "Primordial Black Holes and Quantum Effects," arXiv:1402.1437 [gr-qc].

[30] B. J. Carr, "Primordial black holes: Recent developments," *eConf* **C041213** (2004) 0204, arXiv:astro-ph/0504034 [astro-ph].

[31] M. Y. Khlopov, "Primordial Black Holes," *Res.Astron.Astrophys.* **10** (2010) 495–528, arXiv:0801.0116 [astro-ph].

[32] A. M. Green, "Primordial Black Holes: sirens of the early Universe," arXiv:1403.1198 [gr-qc].

[33] J. M. Bardeen, J. R. Bond, N. Kaiser, and A. S. Szalay, "The statistics of peaks of Gaussian random fields,"ApJ **304** (May, 1986) 15–61.

[34] C. W. Misner and D. H. Sharp, "Relativistic equations for adiabatic, spherically symmetric gravitational collapse," *Phys.Rev.B* **136** (1964) 571–576.

[35] J. C. Niemeyer and K. Jedamzik, "Dynamics of primordial black hole formation," *Phys.Rev.D* **59** (1999) 124013, arXiv:astro-ph/9901292 [astro-ph].

[36] T. W. Baumgarte, S. L. Shapiro, and S. A. Teukolsky, "Computing supernova collapse to neutron stars and black holes," *Astrophys.J. Pt 1* **443** (1995) no. 2, 717–734.

[37] W. C. Hernandez and C. W. Misner, "Observer Time as a Coordinate in Relativistic Spherical Hydrodynamics," *Astrophys.J.* **143** (1966) 452.

[38] M. Shibata and M. Sasaki, "Black hole formation in the Friedmann universe: Formulation and computation in numerical relativity," *Phys.Rev.D* **60** (1999) 084002, arXiv:gr-qc/9905064 [gr-qc].

[39] D. Wands, K. A. Malik, D. H. Lyth, and A. R. Liddle, "A New approach to the evolution of cosmological perturbations on large scales," *Phys.Rev.* **D62** (2000) 043527, arXiv:astro-ph/0003278 [astro-ph].

[40] Y. Tanaka and M. Sasaki, "Gradient expansion approach to nonlinear superhorizon perturbations," *Prog.Theor.Phys.* **117** (2007) 633–654, arXiv:gr-qc/0612191 [gr-qc].

[41] J. C. Niemeyer and K. Jedamzik, "Near-critical gravitational collapse and the initial mass function of primordial black holes," *Phys.Rev.Lett.* **80** (1998) 5481–5484, arXiv:astro-ph/9709072 [astro-ph].

[42] I. Hawke and J. Stewart, "The dynamics of primordial black hole formation," *Class.Quant.Grav.* **19** (2002) 3687–3707.

[43] I. Musco, J. C. Miller, and A. G. Polnarev, "Primordial black hole formation in the radiative era: Investigation of the critical nature of the collapse," *Class.Quant.Grav.* **26** (2009) 235001, arXiv:0811.1452 [gr-qc].

[44] I. Musco and J. C. Miller, "Primordial black hole formation in the early universe: critical behaviour and self-similarity," *Class.Quant.Grav.* **30** (2013) 145009, arXiv:1201.2379 [gr-qc].

[45] I. Musco, J. C. Miller, and L. Rezzolla, "Computations of primordial black hole formation," *Class.Quant.Grav.* **22** (2005) 1405–1424, arXiv:gr-qc/0412063 [gr-qc].

[46] A. G. Polnarev and I. Musco, "Curvature profiles as initial conditions for primordial black hole formation," *Class.Quant.Grav.* **24** (2007) 1405–1432, arXiv:gr-qc/0605122 [gr-qc].

[47] A. Polnarev, T. Nakama, and J. Yokoyama, "Self-consistent initial conditions for primordial black hole formation," *JCAP* **1209** (2012) 027, arXiv:1204.6601 [gr-qc].

[48] J. Hidalgo and A. Polnarev, "Probability of primordial black hole formation and its dependence on the radial profile of initial configurations," *Phys.Rev.* **D79** (2009) 044006, arXiv:0806.2752 [astro-ph].

[49] T. Nakama, T. Harada, A. Polnarev, and J. Yokoyama, "Identifying the most crucial parameters of the initial curvature profile for primordial black hole formation," *JCAP* **2014** (2014) no. 01, 037, arXiv:1310.3007 [gr-qc].

[50] T. Nakama, T. Harada, A. Polnarev, and J. Yokoyama, "Investigating formation condition of primordial black holes for generalized initial perturbation profiles," arXiv:1401.7740 [gr-qc].

[51] R. Wald, *General Relativity*. University Of Chicago Press, 1984.

[52] J. von Neumann and R. Richtmyer, "A Method for the Numerical Calculation of Hydrodynamic Shocks," *Journal of Applied Physics* **21** (1950) no. 3, 232–237.

[53] T. W. Baumgarte and S. L. Shapiro, *Numerical Relativity*. Cambridge University Press, 2010.

[54] T. Harada, C.-M. Yoo, and K. Kohri, "Threshold of primordial black hole formation," *Phys.Rev.* **D88** (2013) no. 8, 084051, arXiv:1309.4201 [astro-ph.CO].

[55] I. Musco, "The threshold for primordial black holes: dependence on the shape of the cosmological perturbations," arXiv:1809.02127 [gr-qc].

[56] J. M. Bardeen, "Gauge Invariant Cosmological Perturbations," *Phys.Rev.* **D22** (1980) 1882–1905.

[57] L. E. Kidder, M. A. Scheel, S. A. Teukolsky, E. D. Carlson, and G. B. Cook, "Black hole evolution by spectral methods," *Phys.Rev.* **D62** (2000) 084032, arXiv:gr-qc/0005056 [gr-qc].

[58] R. Courant, K. Friedrichs, and H. Lewy, "Über die partiellen Differenzengleichungen der mathematischen Physik," *Mathematische Annalen* **100** (1928) no. 1, 32–74. http://dx.doi.org/10.1007/BF01448839.

[59] M. M. May and R. H. White, "Hydrodynamic Calculations of General-Relativistic Collapse," *Phys.Rev.* **141** (1966) 1232–1241.

[60] M. May and R. White, "Stellar Dynamics and Gravitational Collapse," in *Methods in Computational Physics*, B. Alder, S. Fernbach, and M. Rotenberg, eds., vol. 7, ch. 5. Academic Press, NY, USA, 1967.

[61] J. C. Miller and S. Motta, "Computations of spherical gravitational collapse using null slicing," *Classical and Quantum Gravity* **6** (1989) no. 2, 185. http://stacks.iop.org/0264-9381/6/i=2/a=012.